

## Supporting Information

### **Novel Organic-Inorganic Hybrids Based on T<sub>8</sub> and T<sub>10</sub> Silsesquioxanes: Synthesis, Cage-Rearrangement and Properties**

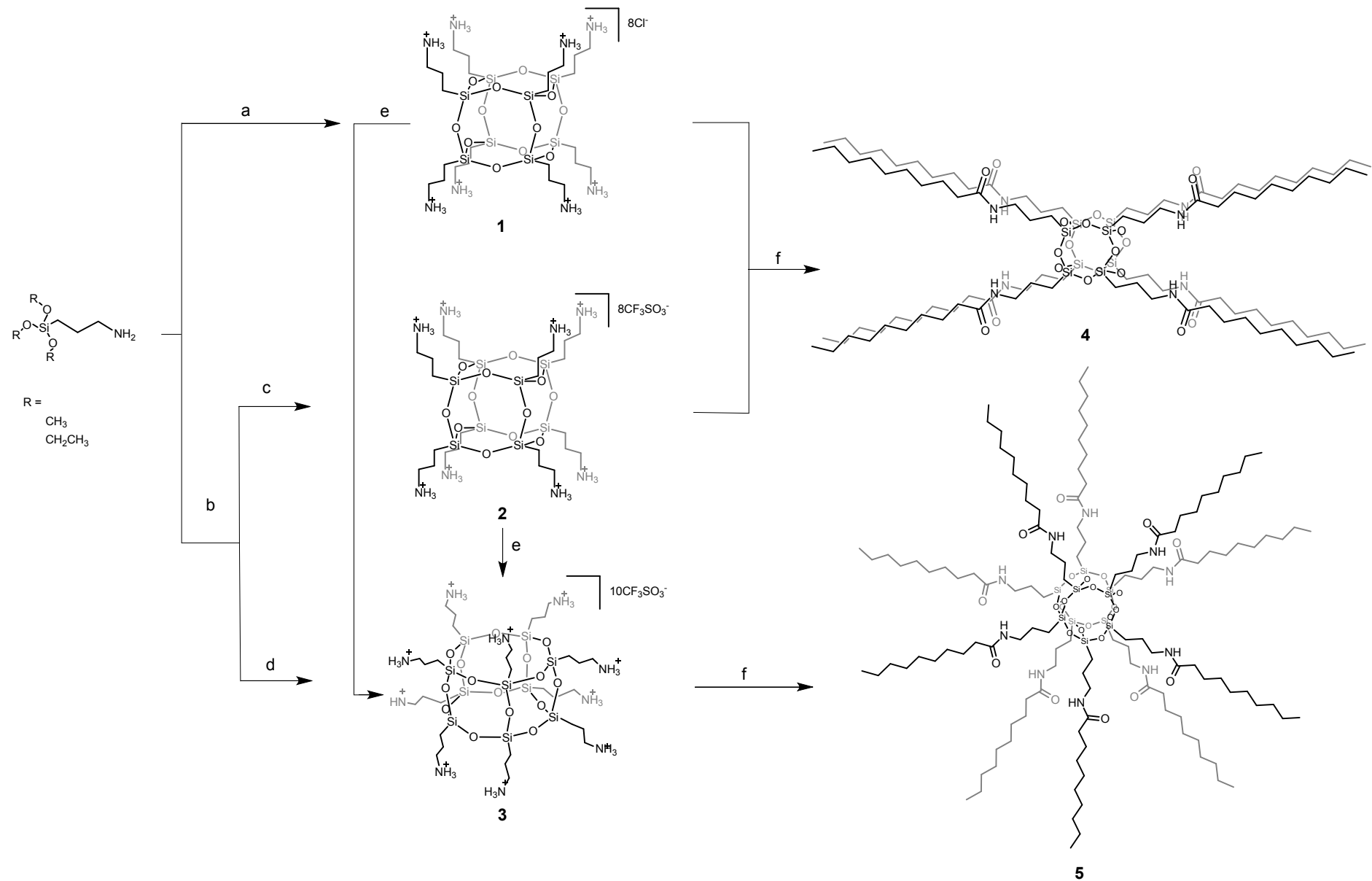
Mateusz Janeta, Łukasz John,\* Jolanta Ejfler and Sławomir Szafert

*Faculty of Chemistry, University of Wrocław, 14 F. Joliot-Curie, 50-383  
Wrocław, Poland*

\*To whom correspondence should be addressed: E-mail: lukasz.john@chem.uni.wroc.pl

<u>Table of Contents</u>	<u>Page</u>
<b>Scheme S1.</b> Synthesis of <b>1–5</b> .	4
<b>Figure S1.</b> Powder XRD patterns for <b>1–5</b> .	5
<b>Figure S2.</b> Powder XRD patterns for <b>1–5</b> after heating to the decomposition temperature.	5
<b>Figure S3.</b> $^1\text{H}$ NMR (500 MHz, DMSO-d <sub>6</sub> , 300 K) spectrum of <b>1</b> .	6
<b>Figure S4.</b> $^{13}\text{C}$ NMR (126 MHz, DMSO-d <sub>6</sub> , 300 K) spectrum of <b>1</b> .	6
<b>Figure S5.</b> $^{29}\text{Si}$ NMR (59.6 MHz, DMSO-d <sub>6</sub> , 300 K) spectrum of <b>1</b> .	7
<b>Figure S6.</b> FT-IR (KBr pellets) spectrum of <b>1</b> .	7
<b>Figure S7.</b> HR-MS (ESI+, TOF, MeOH) spectrum of <b>1</b> .	8
<b>Figure S8.</b> EDS spectrum of <b>1</b> .	8
<b>Figure S9.</b> Powder XRD pattern of <b>1</b> .	9
<b>Figure S10.</b> $^1\text{H}$ NMR (500 MHz, DMSO-d <sub>6</sub> , 300 K) spectrum of <b>2</b> .	10
<b>Figure S11.</b> $^{13}\text{C}$ NMR (126 MHz, DMSO-d <sub>6</sub> , 300 K) spectrum of <b>2</b> .	10
<b>Figure S12.</b> $^{29}\text{Si}$ NMR (59.6 MHz, DMSO-d <sub>6</sub> , 300 K) spectrum of <b>2</b> .	11
<b>Figure S13.</b> FT-IR (KBr pellets) spectrum of <b>2</b> .	11
<b>Figure S14.</b> HR-MS (ESI+, TOF, MeOH) spectrum of <b>2</b> .	12
<b>Figure S15.</b> EDS spectrum of <b>2</b> .	12
<b>Figure S16.</b> Powder XRD pattern of <b>2</b> .	13
<b>Figure S17.</b> $^1\text{H}$ NMR (500 MHz, DMSO-d <sub>6</sub> , 300 K) spectrum of <b>3</b> .	14
<b>Figure S18.</b> $^{13}\text{C}$ NMR (126 MHz, DMSO-d <sub>6</sub> , 300 K) spectrum of <b>3</b> .	14
<b>Figure S19.</b> $^{29}\text{Si}$ NMR (59.6 MHz, DMSO-d <sub>6</sub> , 300 K) spectrum of <b>3</b> (method A).	15
<b>Figure S20.</b> $^{29}\text{Si}$ NMR (59.6 MHz, DMSO-d <sub>6</sub> , 300 K) spectrum of <b>3</b> (method B).	15
<b>Figure S21.</b> $^{29}\text{Si}$ NMR (59.6 MHz, DMSO-d <sub>6</sub> , 300 K) spectrum of <b>3</b> (method C).	16
<b>Figure S22.</b> $^{29}\text{Si}$ NMR (59.6 MHz, DMSO-d <sub>6</sub> , 300 K) spectrum of <b>3</b> (method D).	16
<b>Figure S23.</b> FT-IR (KBr pellets) spectrum of <b>3</b> .	17
<b>Figure S24.</b> HR-MS (ESI+, TOF, MeOH) spectrum of <b>3</b> (method A).	17
<b>Figure S25.</b> HR-MS (ESI+, TOF, MeOH) spectrum of <b>3</b> (method B).	18
<b>Figure S26.</b> HR-MS (ESI+, TOF, MeOH) spectrum of <b>3</b> (method C).	18
<b>Figure S27.</b> HR-MS (ESI+, TOF, MeOH) spectrum of <b>3</b> (method D).	19
<b>Figure S28.</b> EDS spectrum of <b>3</b> .	19
<b>Figure S29.</b> Powder XRD pattern of <b>3</b> .	20
<b>Figure S30.</b> $^1\text{H}$ DOSY (600 MHz, DMSO-d <sub>6</sub> , 300 K) spectrum of <b>2</b> (top) and <b>3</b> (bottom).	20
<b>Figure S31.</b> $^1\text{H}$ NMR (500 MHz, DMSO-d <sub>6</sub> , 300 K) spectrum of <b>4</b> .	21
<b>Figure S32.</b> $^{13}\text{C}$ NMR (126 MHz, CDCl <sub>3</sub> , 300 K) spectrum of <b>4</b> .	21
<b>Figure S32.</b> $^1\text{H}$ - $^1\text{H}$ COSY NMR (500 MHz, DMSO-d <sub>6</sub> , 300 K) spectrum of <b>4</b> .	22
<b>Figure S34.</b> $^1\text{H}$ DOSY (600 MHz, CDCl <sub>3</sub> , 300 K) spectrum of <b>4</b> .	22
<b>Figure S35.</b> $^{29}\text{Si}$ NMR (59.6 MHz, DMSO-d <sub>6</sub> , 300 K) spectrum of <b>4</b> .	23
<b>Figure S36.</b> FT-IR (KBr pellets) spectrum of <b>4</b> .	23
<b>Figure S37.</b> HR-MS (ESI+, TOF, CHCl <sub>3</sub> ) spectrum of <b>4</b> .	24

<b>Figure S38.</b> EDS spectrum of <b>4</b> .	24
<b>Figure S39.</b> Powder XRD pattern of <b>4</b> .	25
<b>Figure S40.</b> $^1\text{H}$ NMR (500 MHz, DMSO-d <sub>6</sub> , 300 K) spectrum of <b>5</b> .	26
<b>Figure S41.</b> $^{13}\text{C}$ NMR (126 MHz, CDCl <sub>3</sub> , 300 K) spectrum of <b>5</b> .	26
<b>Figure S42.</b> $^1\text{H}$ DOSY (600 MHz, CDCl <sub>3</sub> , 300 K) spectrum of <b>5</b> .	27
<b>Figure S43.</b> $^{29}\text{Si}$ NMR (59.6 MHz, DMSO-d <sub>6</sub> , 300 K) spectrum of <b>5</b> .	27
<b>Figure S44.</b> FT-IR (KBr pellets) spectrum of <b>5</b> .	28
<b>Figure S45.</b> HR-MS (ESI+, TOF, CHCl <sub>3</sub> ) spectrum of <b>5</b> (method A).	29
<b>Figure S46.</b> HR-MS (ESI+, TOF, CHCl <sub>3</sub> ) spectra of <b>4</b> and <b>5</b> before and after separation.	29
<b>Figure S47.</b> EDS spectrum of <b>5</b> .	30
<b>Figure S48.</b> Powder XRD pattern of <b>5</b> .	30
<b>Figure S49.</b> $^1\text{H}$ NMR (500 MHz, CDCl <sub>3</sub> , 300 K) spectrum of <b>6</b> .	31
<b>Figure S50.</b> $^{13}\text{C}$ NMR (126 MHz, CDCl <sub>3</sub> , 300 K) spectrum of <b>6</b> .	31
<b>Figure S51.</b> TG (black line), and DTA (blue line) thermogram of <b>1</b> .	32
<b>Figure S52.</b> TG (black line), and DTA (blue line) thermogram of <b>2</b> .	32
<b>Figure S53.</b> TG (black line), and DTA (blue line) thermogram of <b>3</b> .	33
<b>Figure S54.</b> TG (black line), and DTA (blue line) thermogram of <b>4</b> (air and nitrogen).	33
<b>Figure S55.</b> TG (black line), and DTA (blue line) thermogram of <b>5</b> (air and nitrogen).	34
<b>Figure S56.</b> TG (black line), and DTA (blue line) thermogram of <b>6</b> (air and nitrogen).	34
<b>Figure S57.</b> First derivative of TG (DTG) thermograms of <b>1–6</b> .	35
<b>Figure S58.</b> DSC of <b>5</b> , 2 <sup>nd</sup> heat and cooling cycle (in nitrogen).	35
<b>Figure S59.</b> DSC of <b>6</b> , 2 <sup>nd</sup> heat and cooling cycle (in nitrogen).	35
<b>Figure S60.</b> Selected HR-TEM images of <b>4</b> (a) and <b>5</b> (b).	36
<b>Figure S61.</b> $^{29}\text{Si}$ NMR (59.6 MHz, DMSO-d <sub>6</sub> , 300 K) spectrum of <b>1</b> after reaction with 0, 1, 4, 8, 12 and 16 equivalents of CH <sub>3</sub> SO <sub>3</sub> H.	37
<b>Figure S62.</b> HR-MS (ESI+, TOF, MeOH) spectra of <b>C</b> .	38
<b>Figure S63.</b> HR-MS (ESI+, TOF, MeOH) spectra of <b>D</b> .	38
<b>Figure S64.</b> HR-MS (ESI+, TOF, MeOH) spectra of <b>E</b> .	39
<b>Figure S65.</b> Molecular models of compound <b>4</b> (a), compound <b>5</b> (b).	39
<b>Table S1.</b> MM2 calculations of the minimization energies of Compound <b>2</b> , <b>3</b> , <b>4</b> , <b>5</b> .	39
<b>Figure S66.</b> $^{29}\text{Si}$ NMR (59.63 MHz, DMSO-d <sub>6</sub> , 300 K) spectrum of DSS and TMS.	40



**Scheme S1.** Synthesis of 1–5.

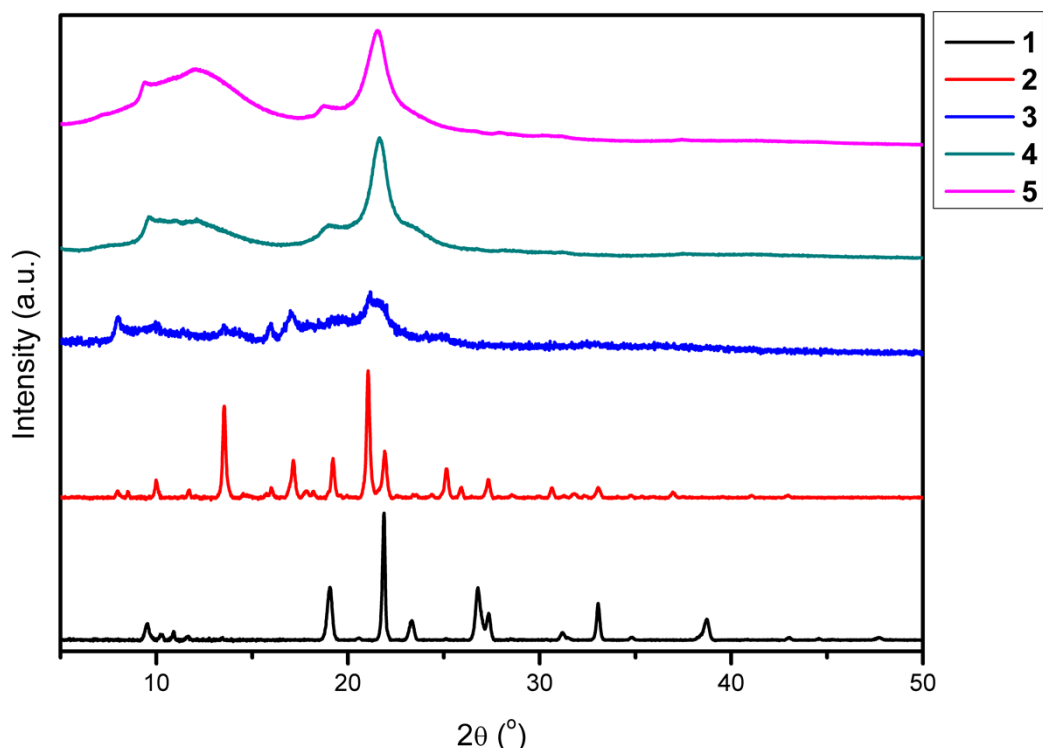


**Figure S1.** Powder XRD patterns for **1–5**.

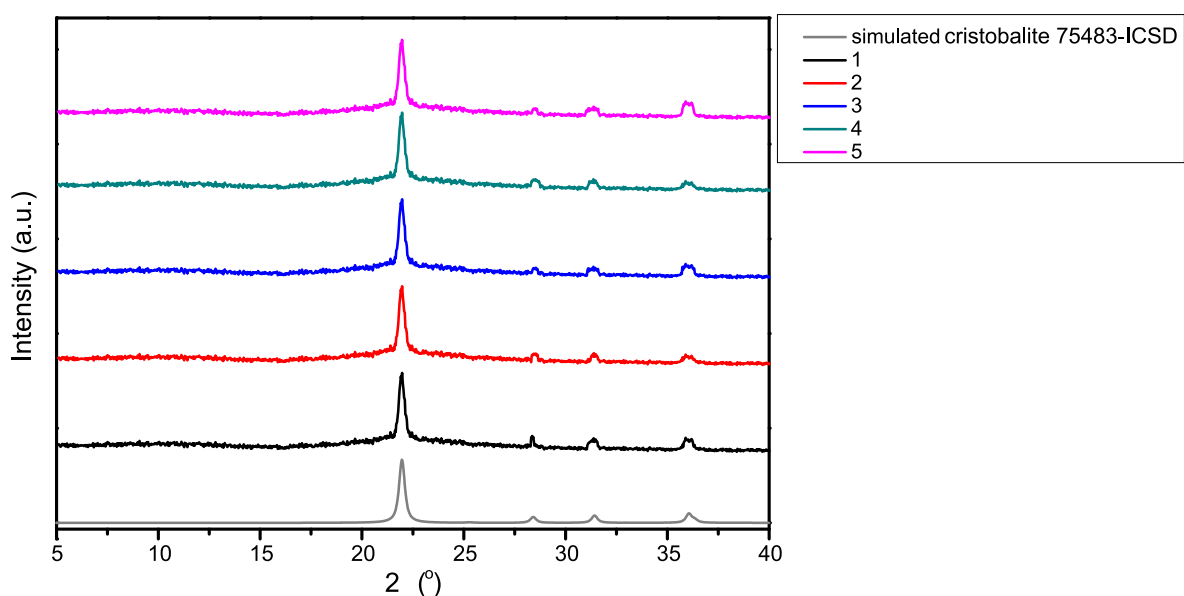


**Figure S2.** Powder XRD patterns for **1–5** after heating to the decomposition temperature.

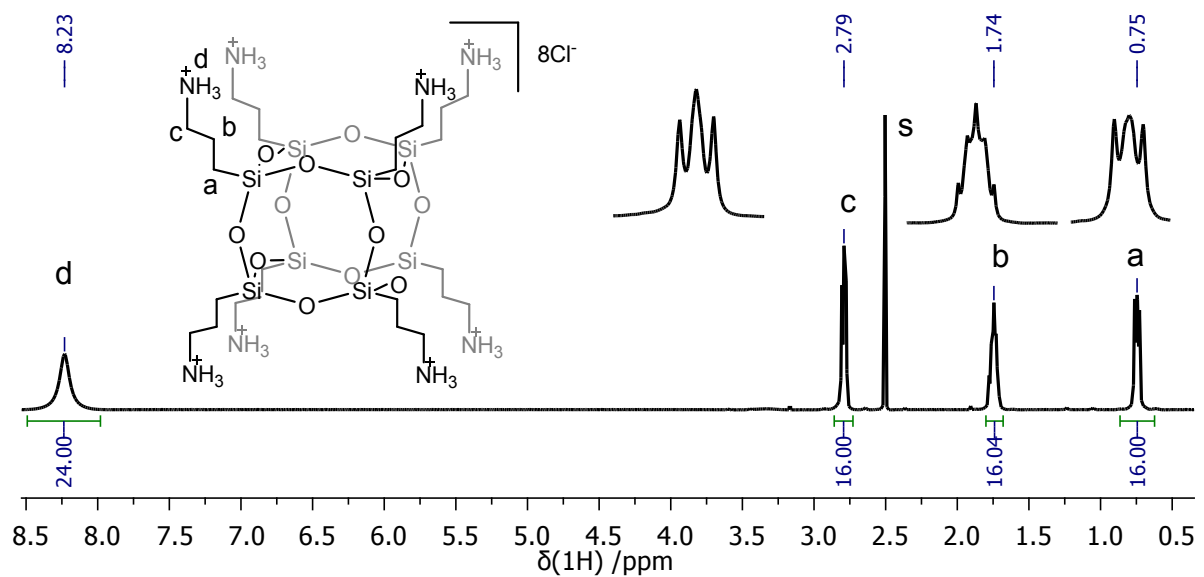


**Figure S3.**  $^1\text{H}$  NMR (500 MHz,  $\text{DMSO-d}_6$ , 300 K) spectrum of **1**, s = solvent.

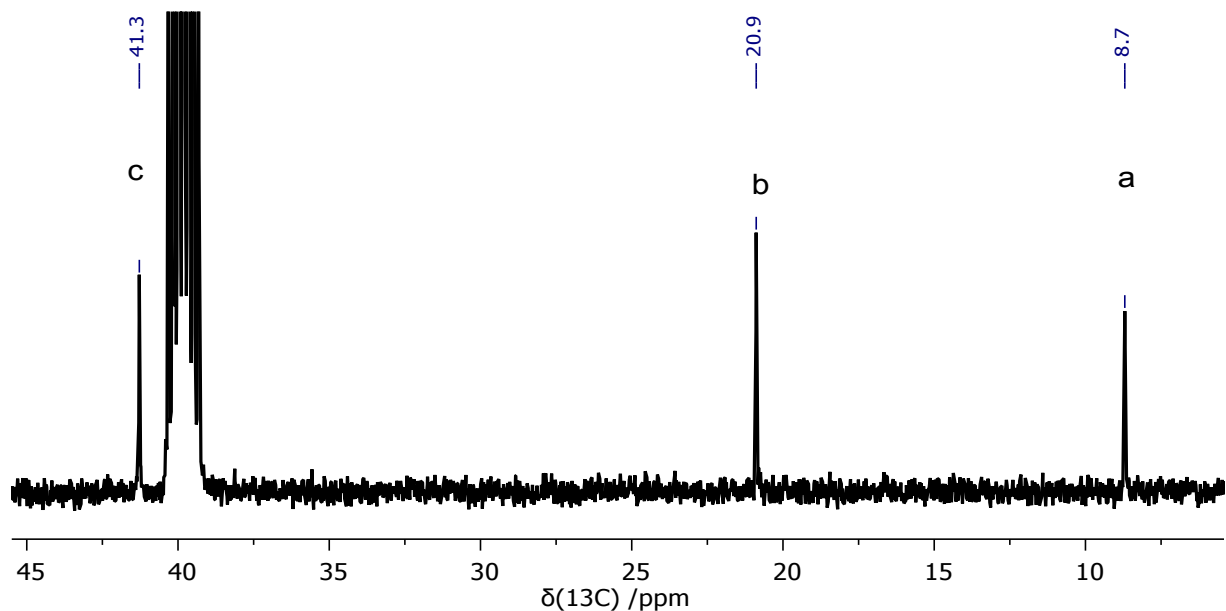


**Figure S4.**  $^{13}\text{C}$  NMR (126 MHz,  $\text{DMSO-d}_6$ , 300 K) spectrum of **1**.

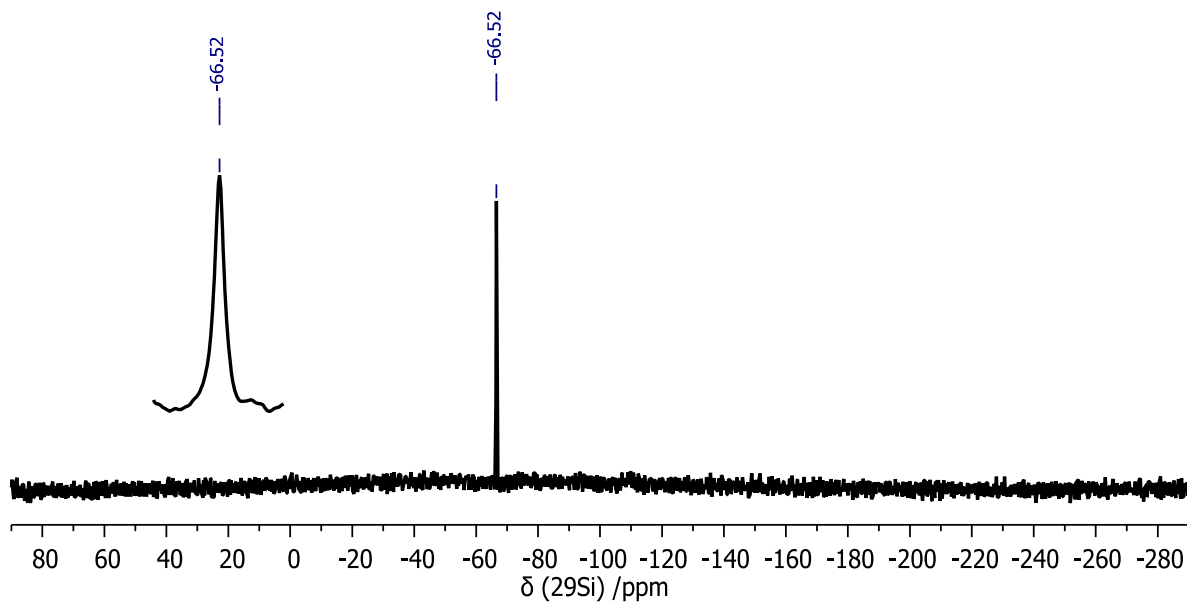


**Figure S5.**  $^{29}\text{Si}$  NMR (59.6 MHz,  $\text{DMSO-d}_6$ , 300 K) spectrum of **1**.

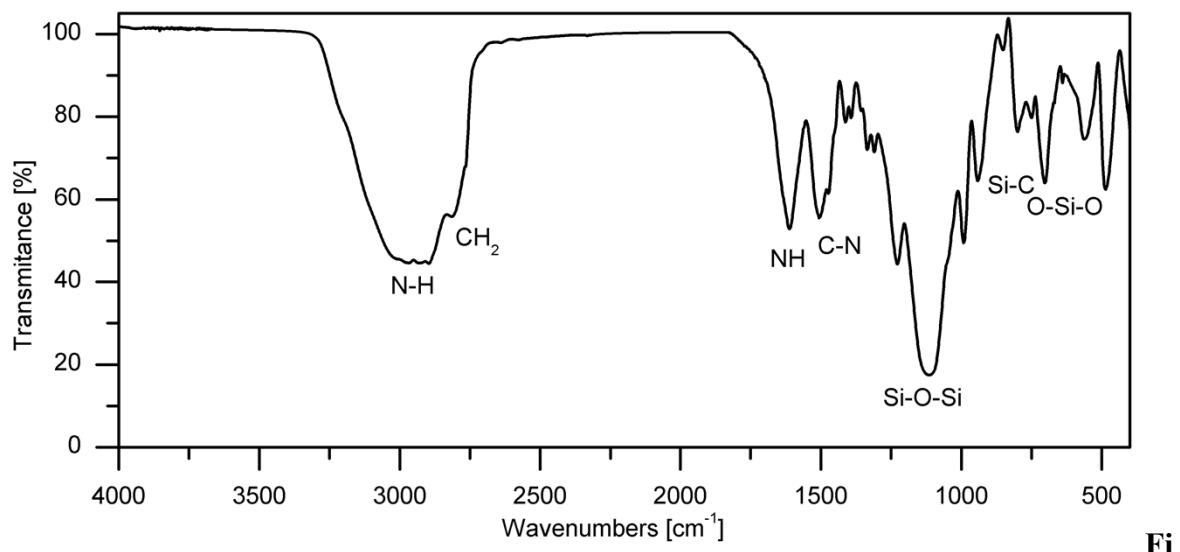


**Figure S6.** FT-IR (KBr pellets) spectrum of **1**.

**Fi**

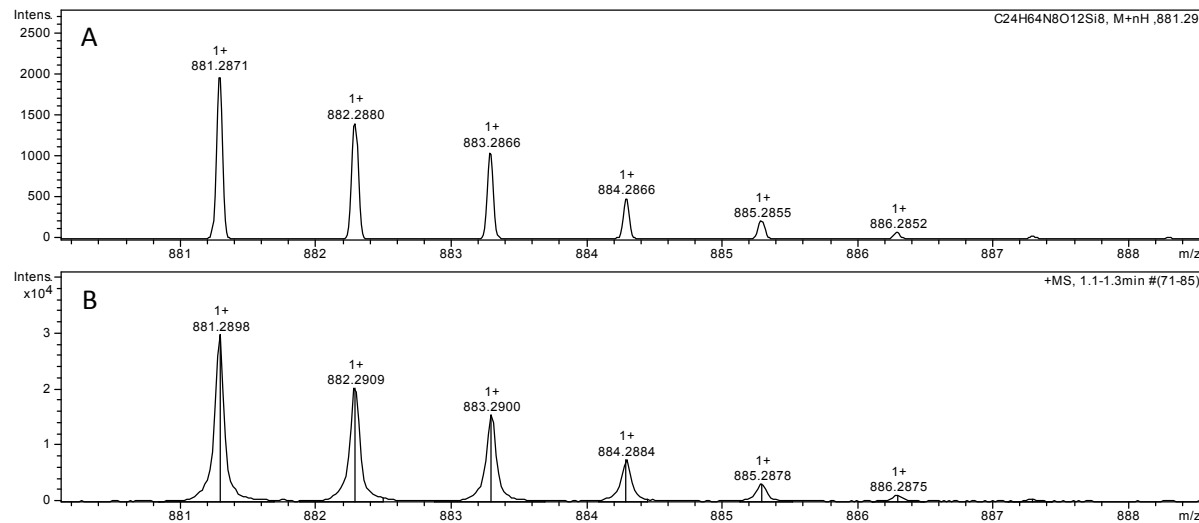


**Figure S7.** Simulated (**A**) calcd for  $\text{C}_{24}\text{H}_{65}\text{N}_8\text{O}_{12}\text{Si}_8$ ,  $[\text{M} - 8\text{HCl} + \text{H}]^+$  and measured (**B**) HR-MS (ESI+, TOF, MeOH) spectra of **1**.

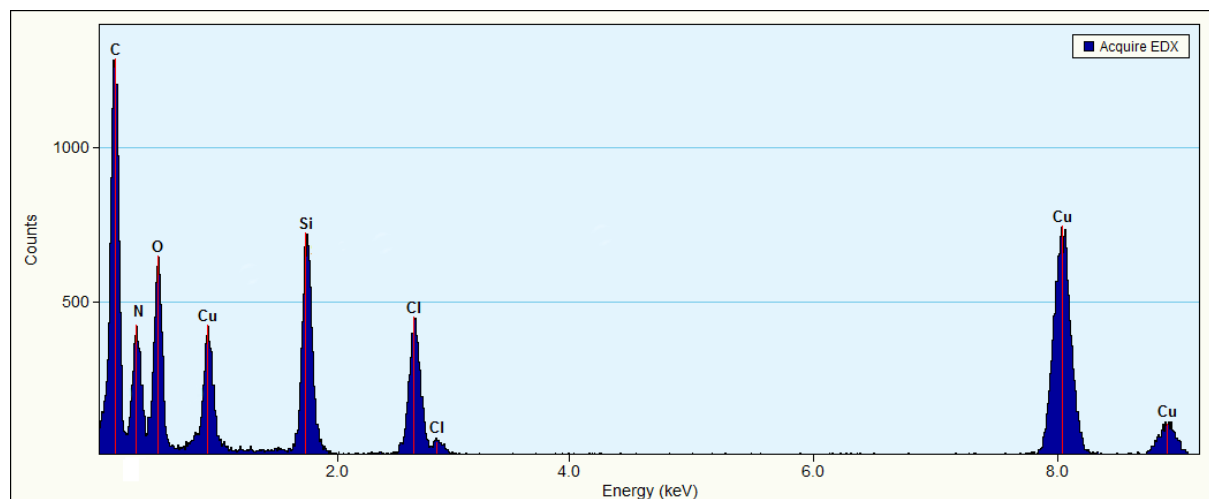


**Figure S8.** EDS spectrum of **1** (copper content is derived from the high-purity conducting Cu grid).

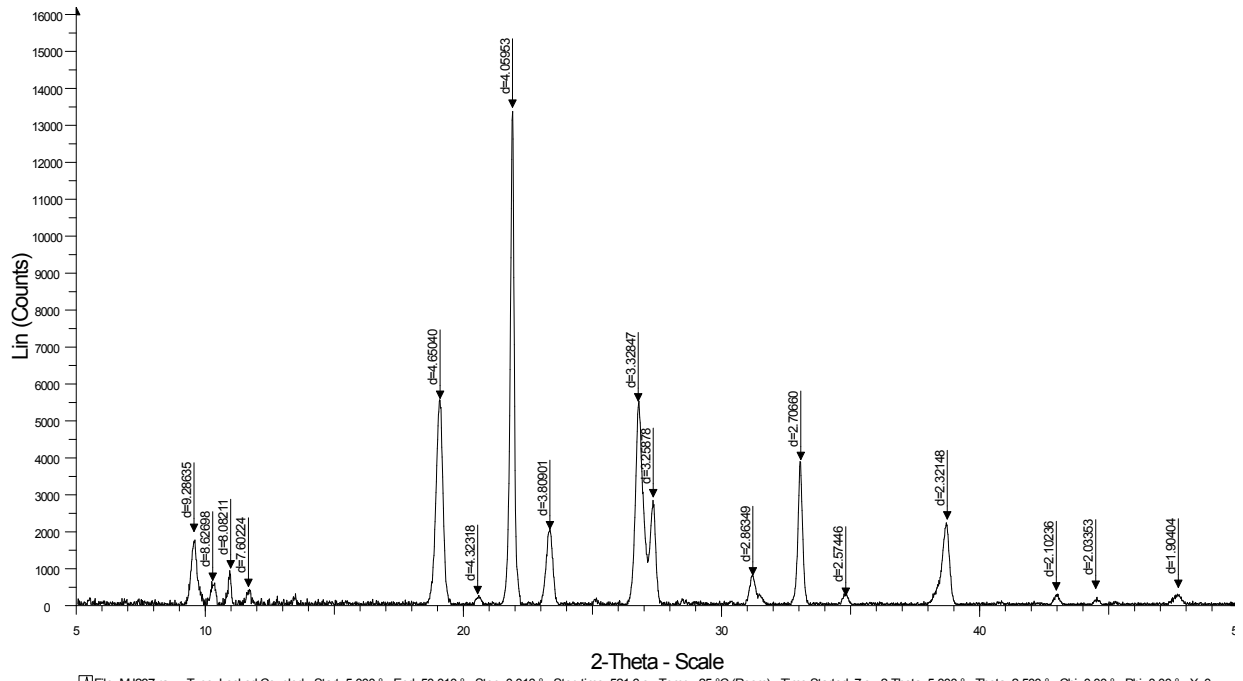


**Figure S9.** Powder XRD pattern of **1**.

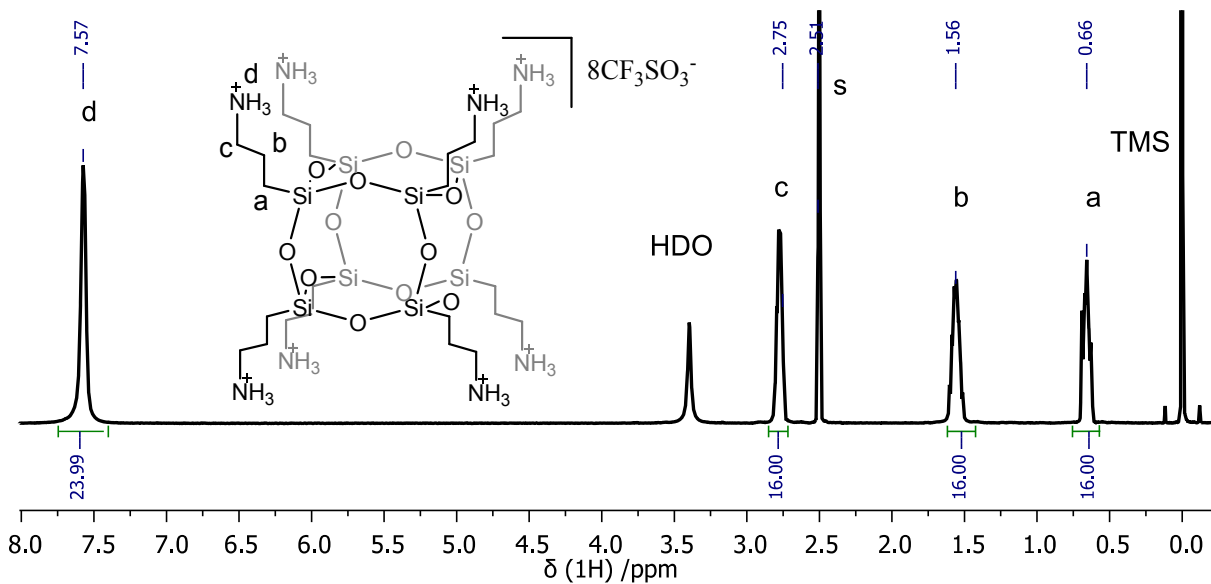


**Figure S10.**  $^1\text{H}$  NMR (500 MHz, DMSO-d<sub>6</sub>, 300 K) spectrum of **2**, s = solvent. Chemical shifts were referenced to tetramethylsilane (TMS) ( $\delta$  0.0).

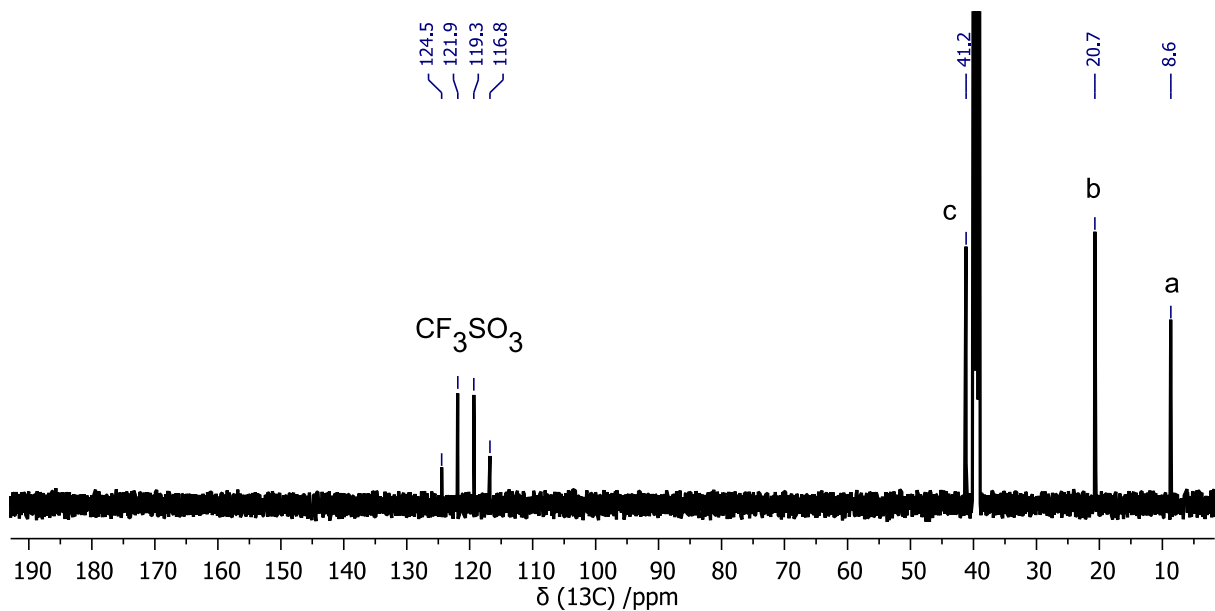


**Figure S11.**  $^{13}\text{C}$  NMR (126 MHz, DMSO-d<sub>6</sub>, 300 K) spectrum of **2**.

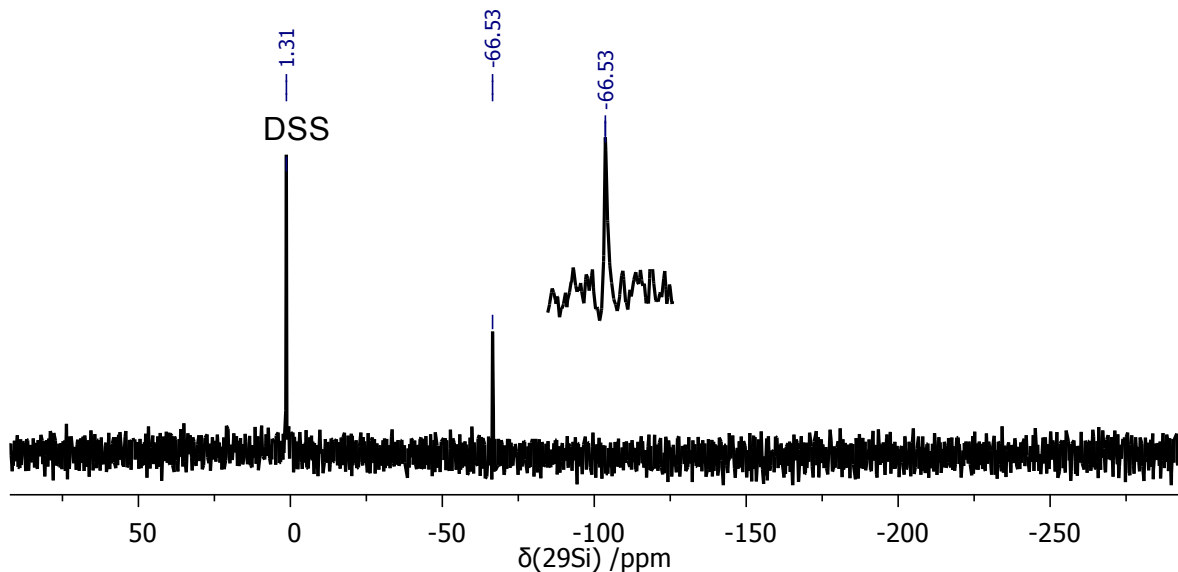


**Figure S12.**  $^{29}\text{Si}$  NMR (59.6 MHz,  $\text{DMSO-d}_6$ , 300 K) spectrum of **2**. Chemical shifts were referenced to 4,4-dimethyl-4-silapentane-1-sulfonic acid (DSS) ( $\delta$  1.316).

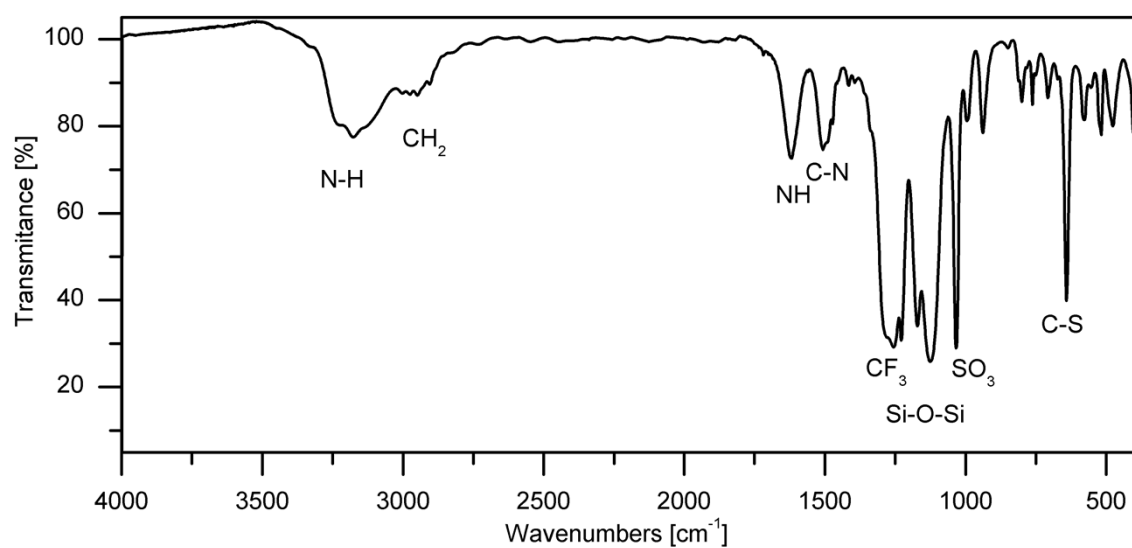


**Figure S13.** FT-IR (KBr pellets) spectrum of **2**.

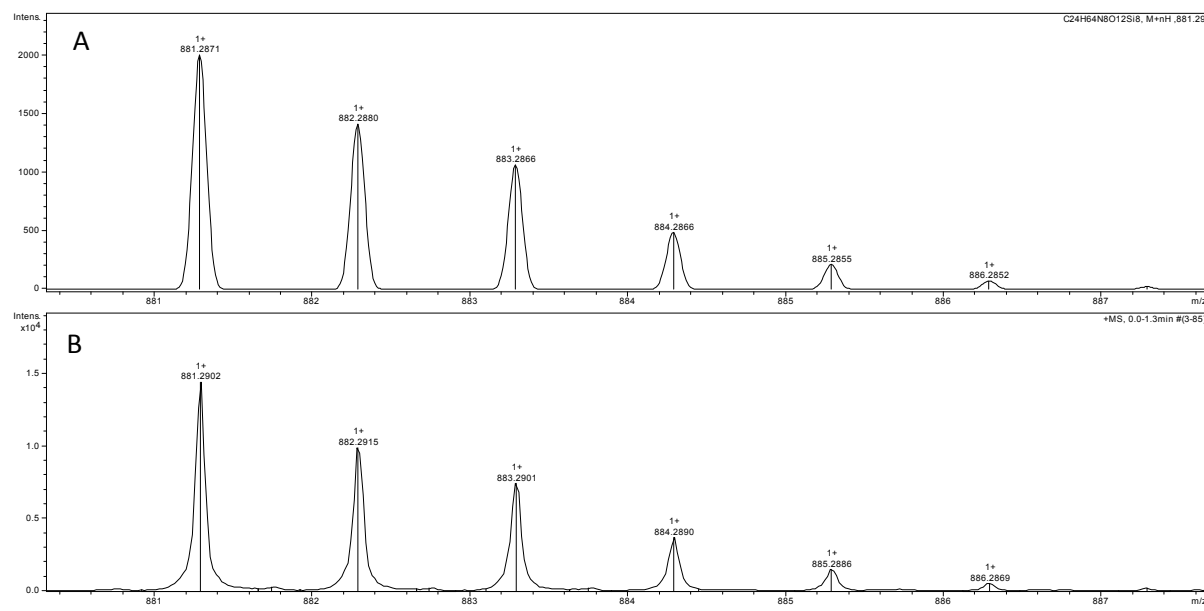


**Figure S14.** Simulated (A) calcd for  $C_{24}H_{65}N_8O_{12}Si_8$ ,  $[M -8CF_3SO_3H + H]^+$  and measured (B) HR-MS (ESI+, TOF, MeOH) spectra of **2**.

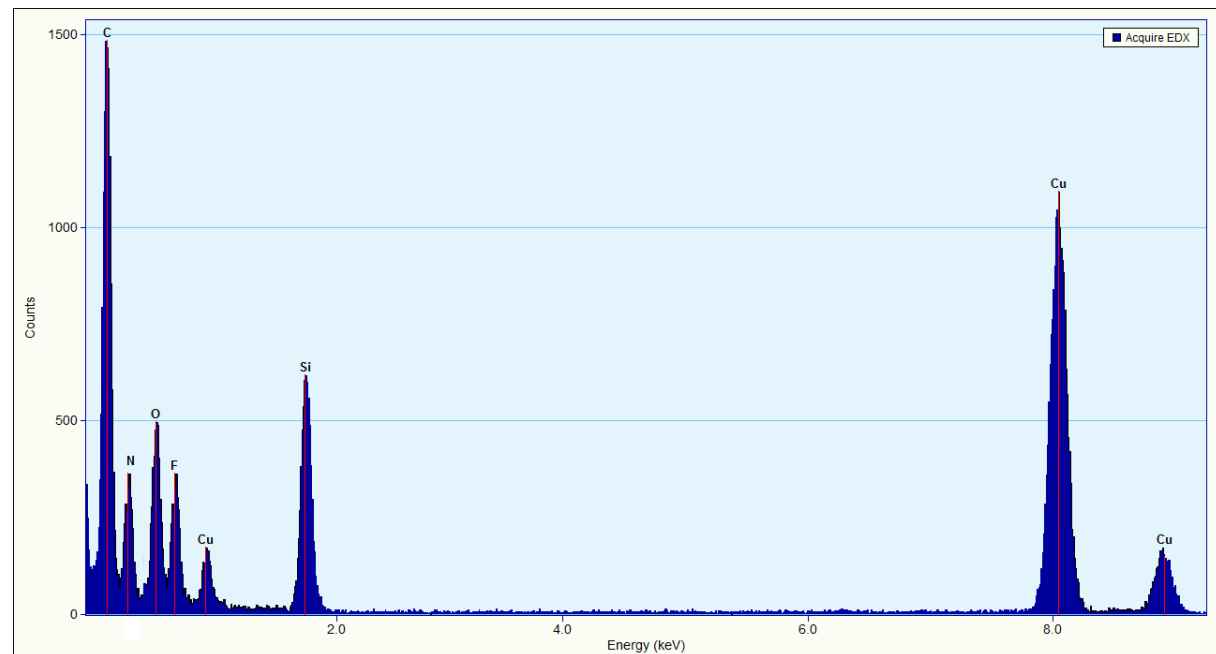


**Figure S15.** EDS spectrum of **2** (copper content is derived from the high-purity conducting Cu grid).

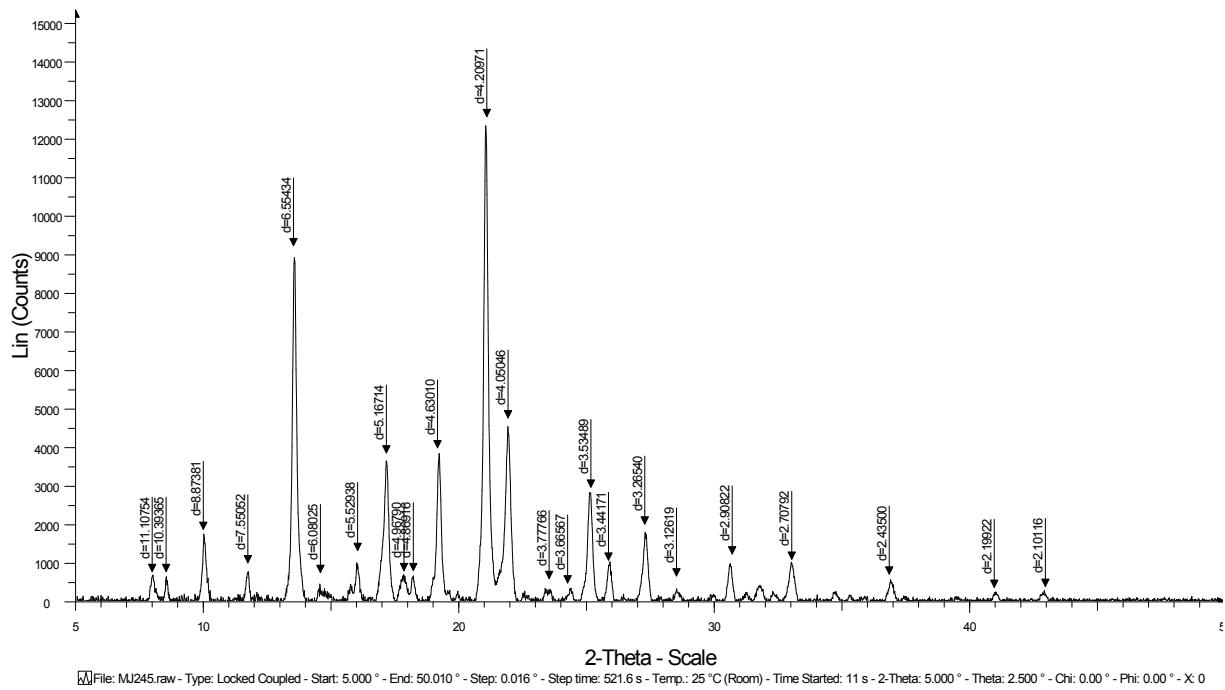


**Figure S16.** Powder XRD pattern of **2**.

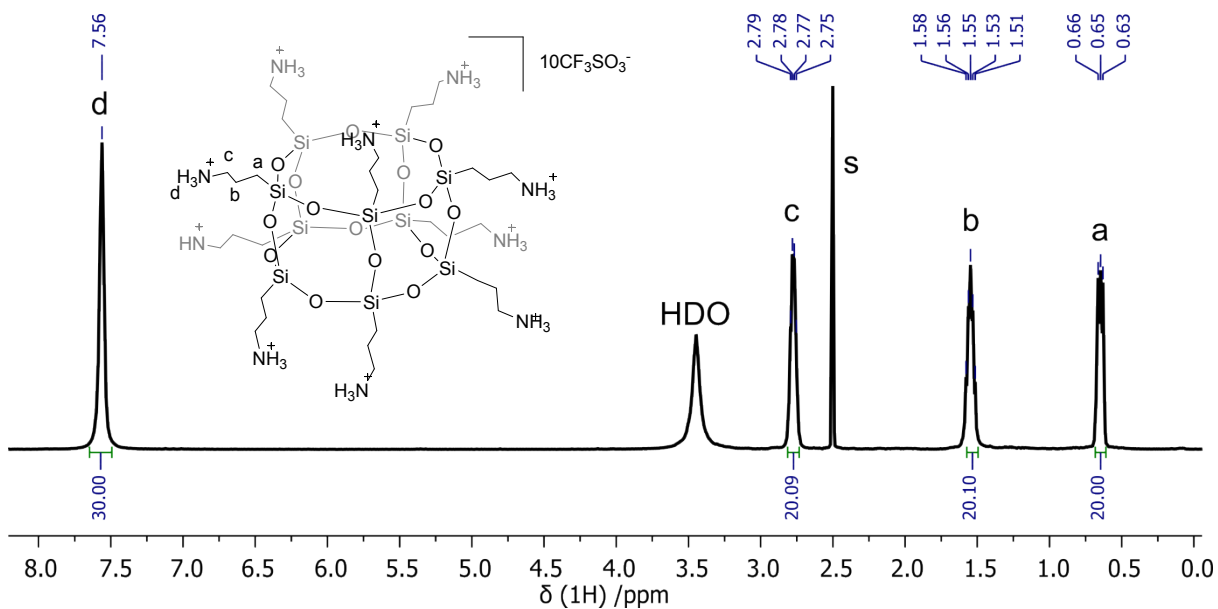


**Figure S17.**  $^1\text{H}$  NMR (500 MHz, DMSO-d<sub>6</sub>, 300 K) spectrum of **3**, s = solvent.

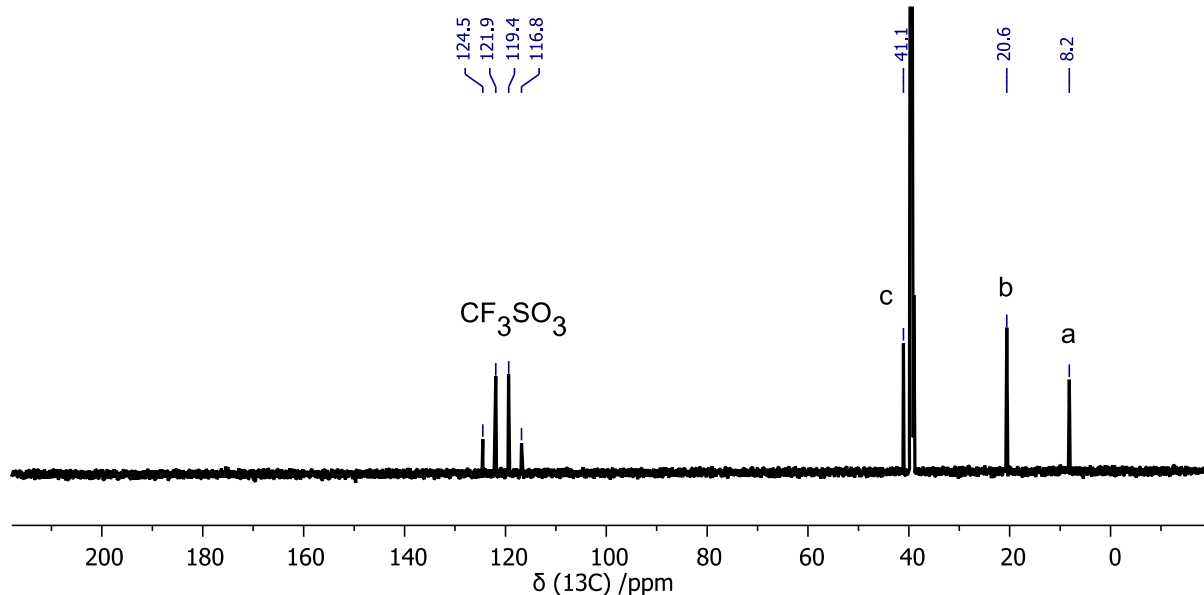


**Figure S18.**  $^{13}\text{C}$  NMR (126 MHz, DMSO-d<sub>6</sub>, 300 K) spectrum of **3**.

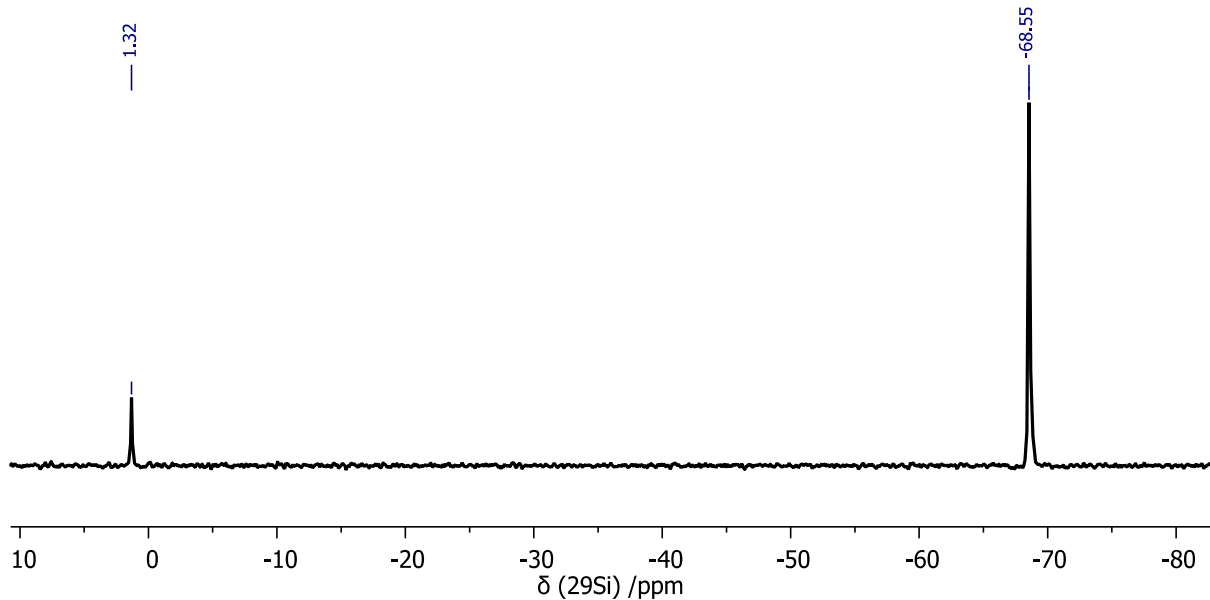


**Figure S19.**  $^{29}\text{Si}$  NMR (59.6 MHz, DMSO-d<sub>6</sub>, 300 K) spectrum of **3** obtained in method A. Chemical shifts were referenced to 4,4-dimethyl-4-silapentane-1-sulfonic acid (DSS) ( $\delta$  1.316).

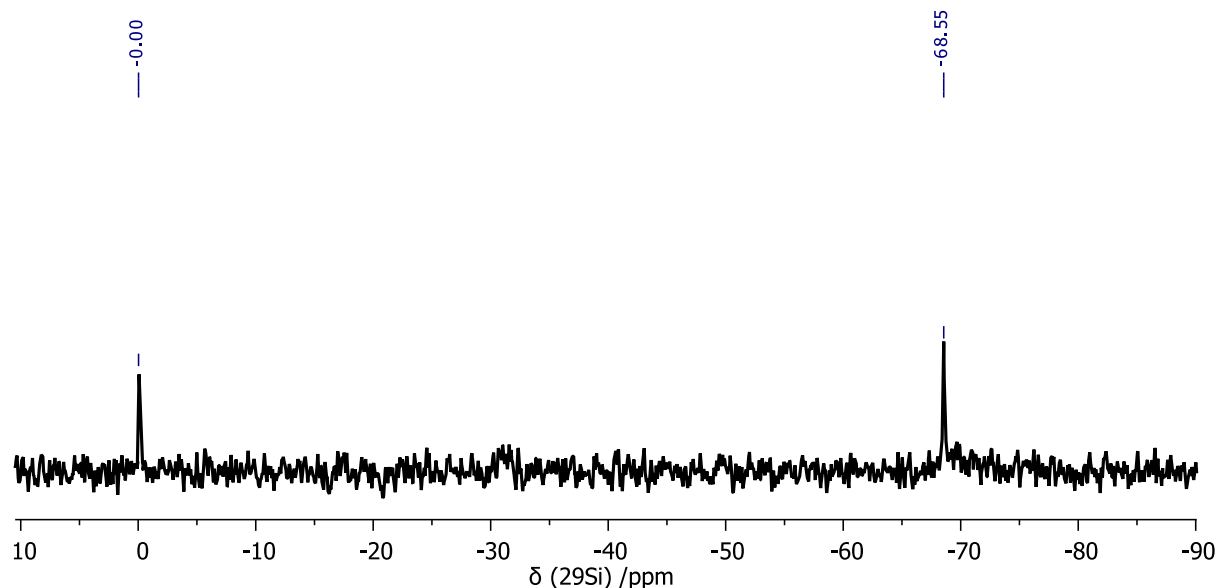


**Figure S20.**  $^{29}\text{Si}$  NMR (59.6 MHz, DMSO-d<sub>6</sub>, 300 K) spectrum of **3** obtained in method B. Chemical shifts were referenced to 4,4-dimethyl-4-silapentane-1-sulfonic acid (DSS) ( $\delta$  1.316).

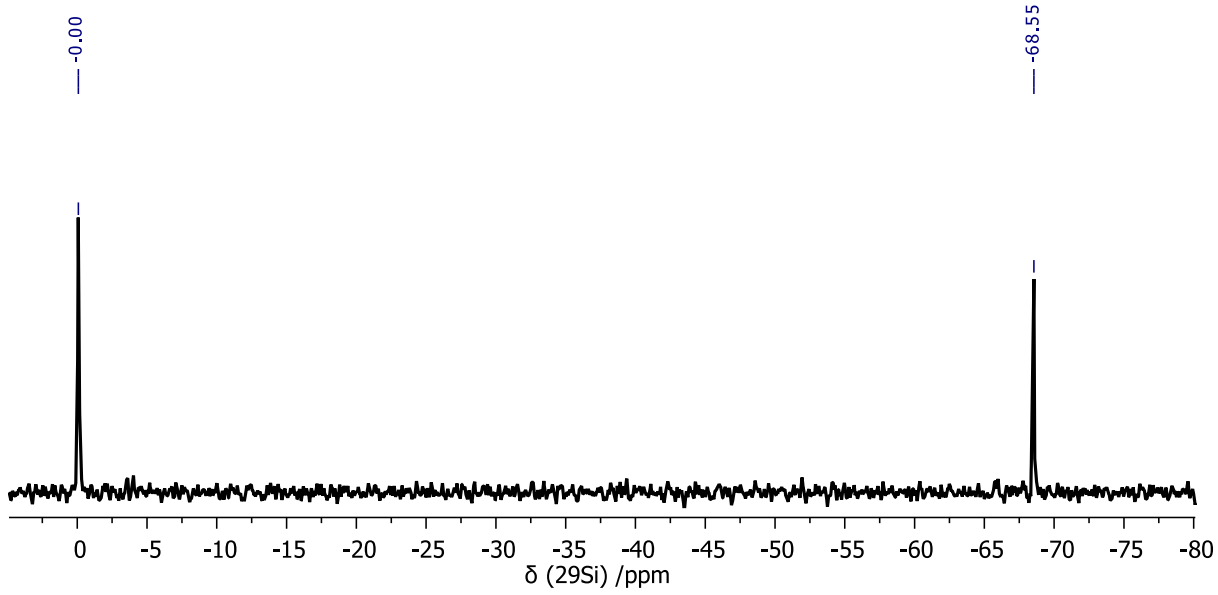


**Figure S21.**  $^{29}\text{Si}$  NMR (59.6 MHz, DMSO- $d_6$ , 300 K) spectrum of **3** obtained in method C (by cage-rearrangement **1**  $\rightarrow$  **3**). Chemical shifts were referenced to tetramethylsilane (TMS) ( $\delta$  0.00).

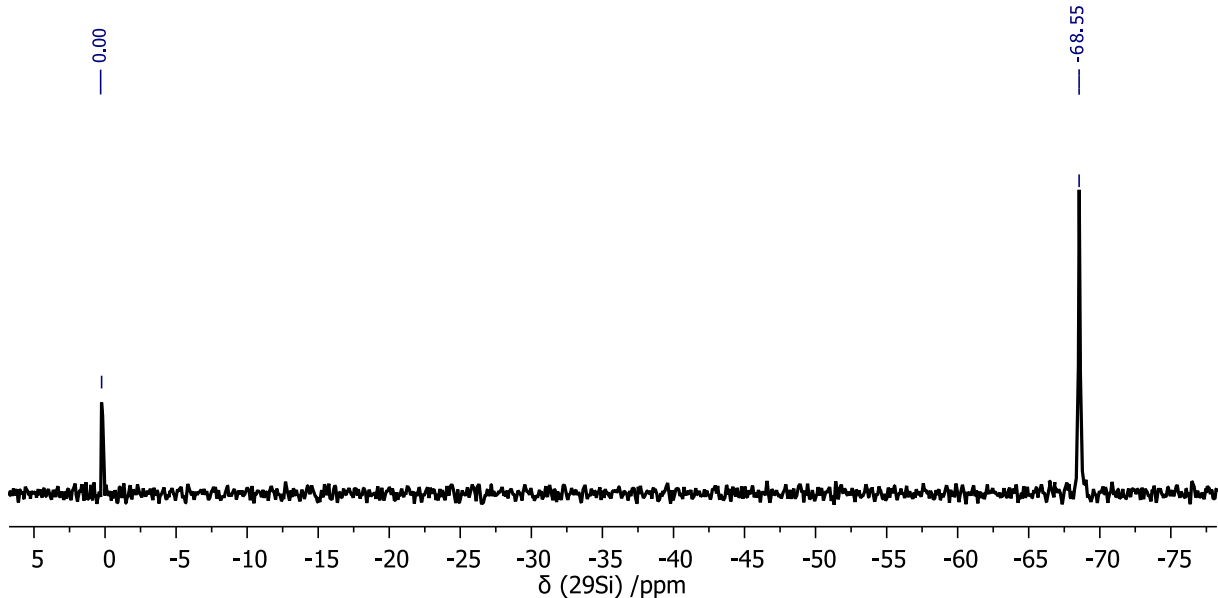


**Figure S22.**  $^{29}\text{Si}$  NMR (59.6 MHz, DMSO- $d_6$ , 300 K) spectrum of **3** obtained in method D (by cage-rearrangement **2**  $\rightarrow$  **3**). Chemical shifts were referenced to tetramethylsilane (TMS) ( $\delta$  0.00).

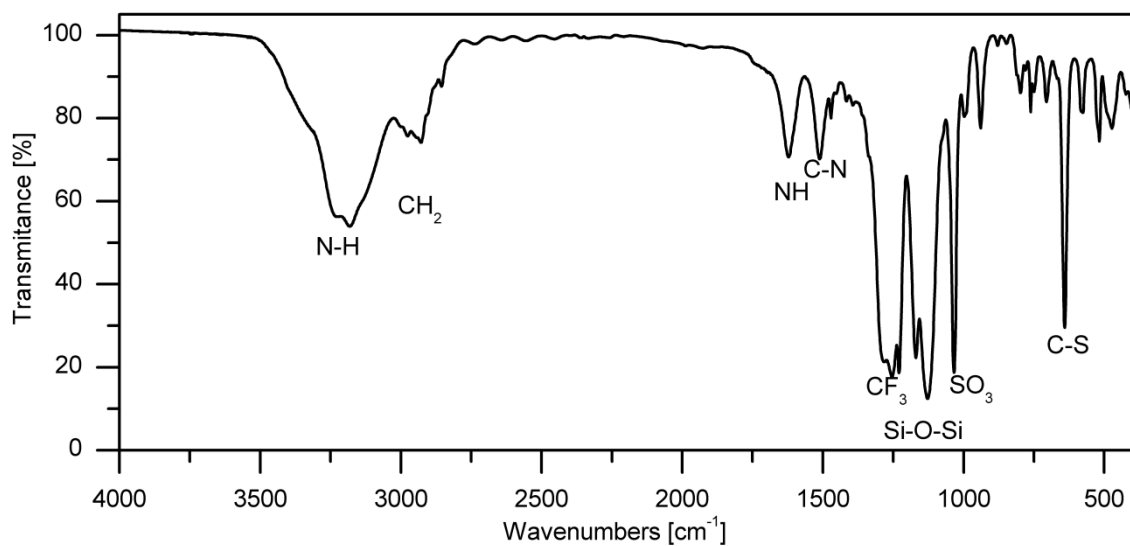


**Figure S23.** FT-IR (KBr pellets) spectrum of **3**.

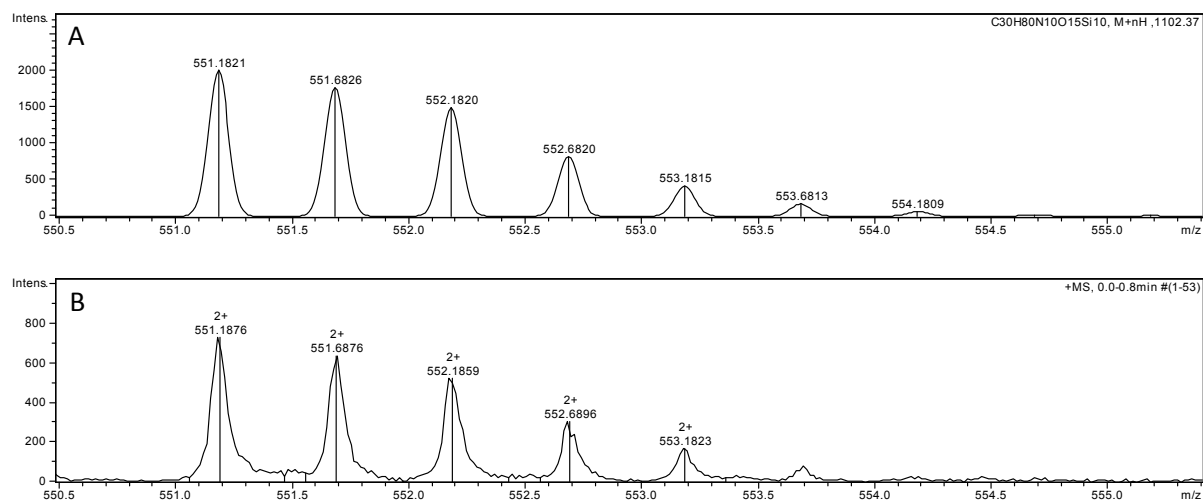


**Figure S24.** Simulated (**A**) calcd for  $C_{30}H_{82}N_{10}O_{15}Si_{10}$ ,  $[M - 10CF_3SO_3H + 2H]^{2+}$  and measured (**B**) HR-MS (ESI+, TOF, MeOH) spectra of **3** obtained in method A.

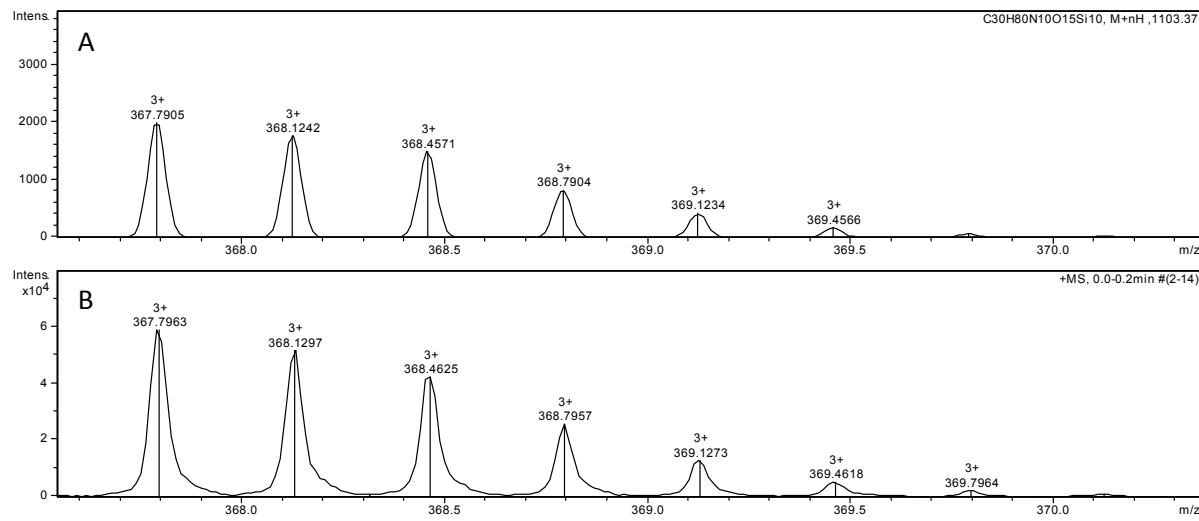


**Figure S25.** Simulated (**A**) calcd for  $\text{C}_{30}\text{H}_{80}\text{N}_{10}\text{O}_{15}\text{Si}_{10}$ ,  $[\text{M} - 10\text{CF}_3\text{SO}_3\text{H} + 3\text{H}]^{3+}$  and measured (**B**) HR-MS (ESI+, TOF, MeOH) spectra of **3** obtained in method B.

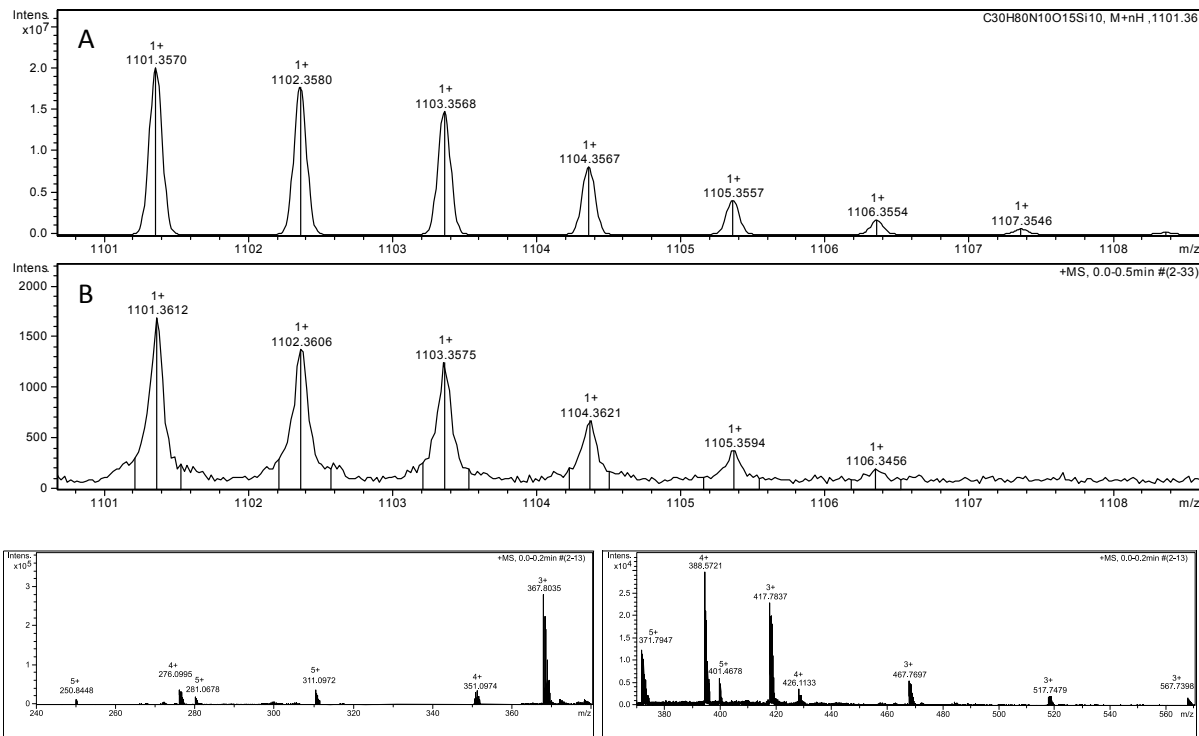


**Figure S26.** HR-MS (ESI+, TOF, MeOH) spectra of **3** obtained in method C (by cage-rearrangement **1**  $\rightarrow$  **3**). Simulated (**A**) calcd for  $\text{C}_{30}\text{H}_{81}\text{N}_{10}\text{O}_{15}\text{Si}_{10}$ ,  $[\text{M} - 10\text{CF}_3\text{SO}_3\text{H} + 1\text{H}]^+$  and measured (**B**).

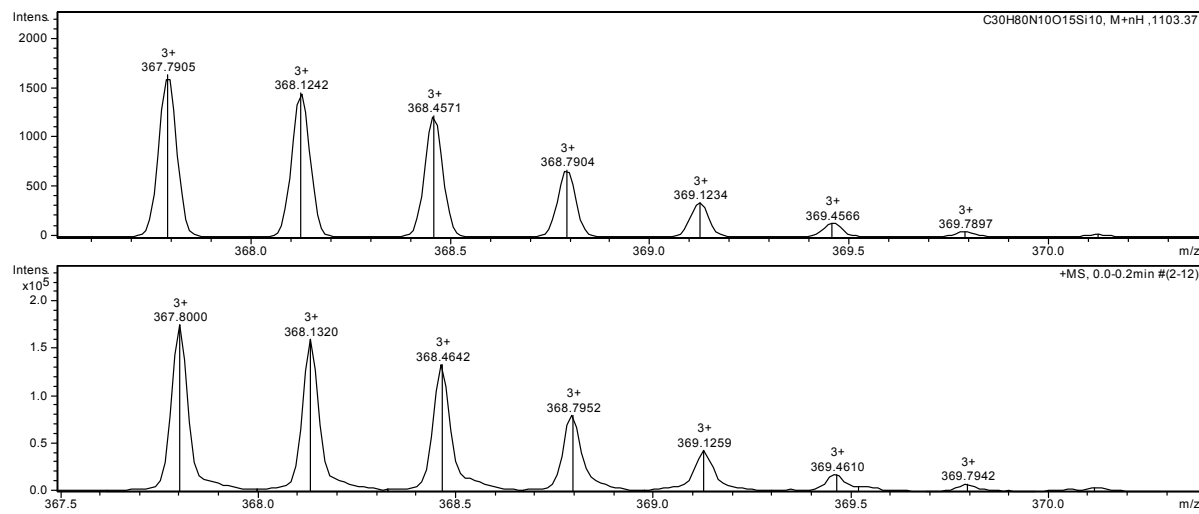


**Figure S27.** HR-MS (ESI+, TOF, MeOH) spectra of **3** obtained in method D (by cage-rearrangement **2** → **3**).

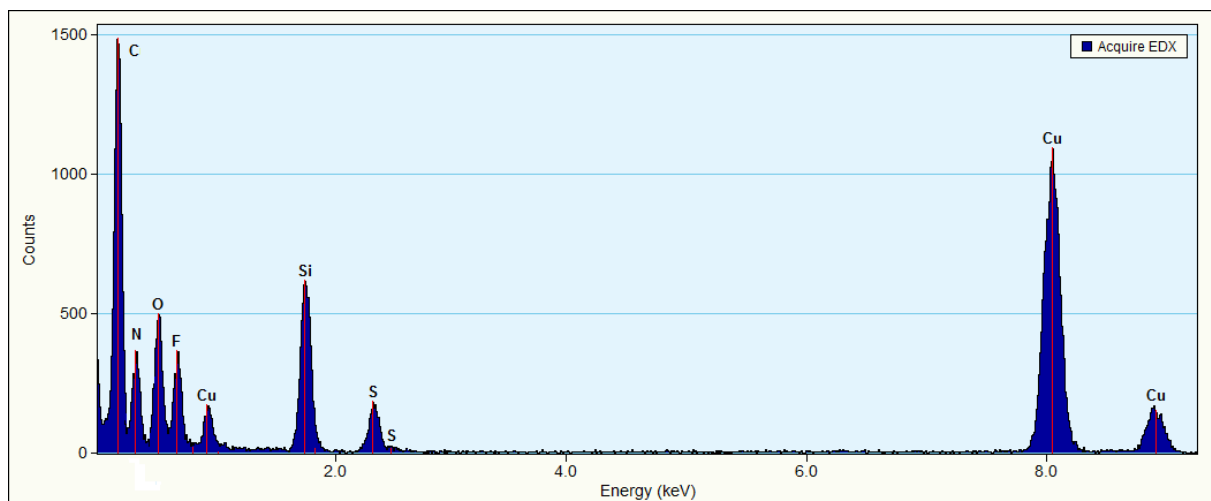


**Figure S28.** EDS spectrum of **3** (copper content is derived from the high-purity conducting Cu grid).

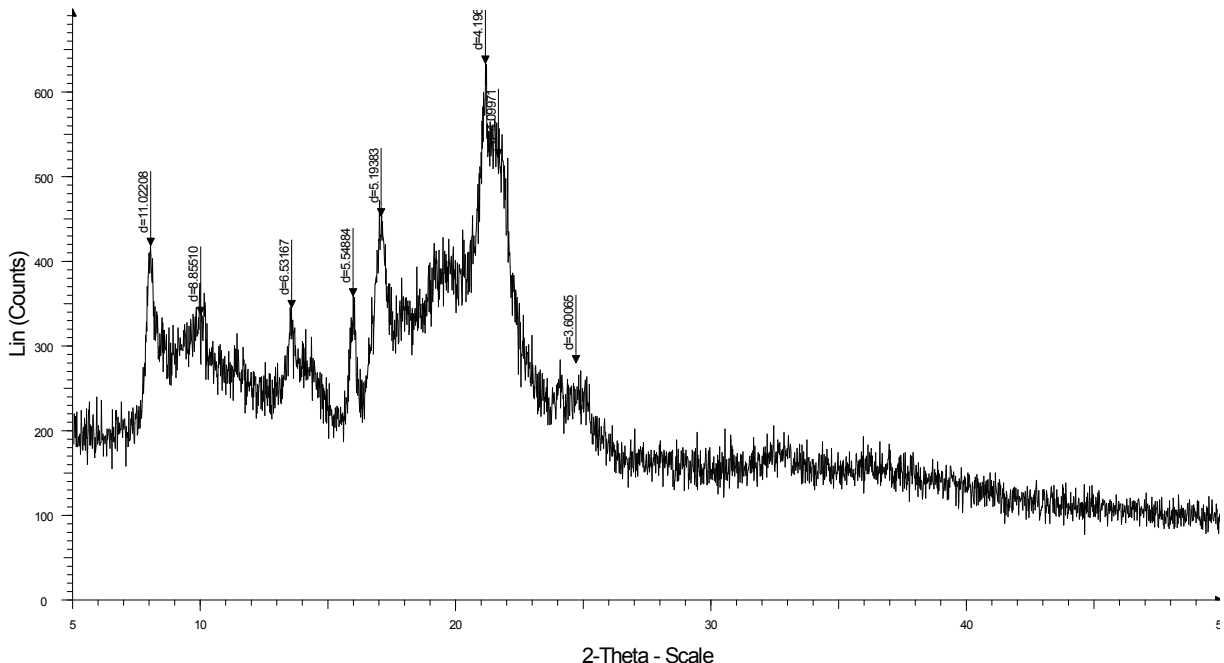


**Figure S29.** Powder XRD pattern of **3**.

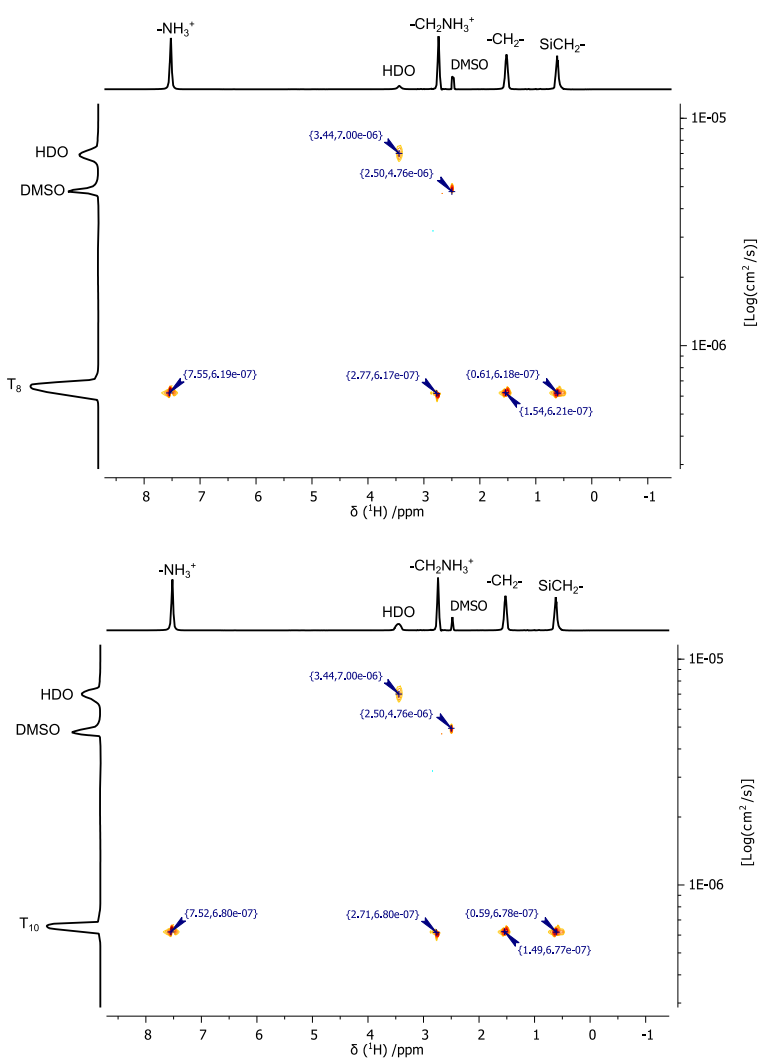


**Figure S30.**  $^1\text{H}$  DOSY (600 MHz,  $\text{DMSO-d}_6$ , 300 K) spectrum of **2** (top) and **3** (bottom).

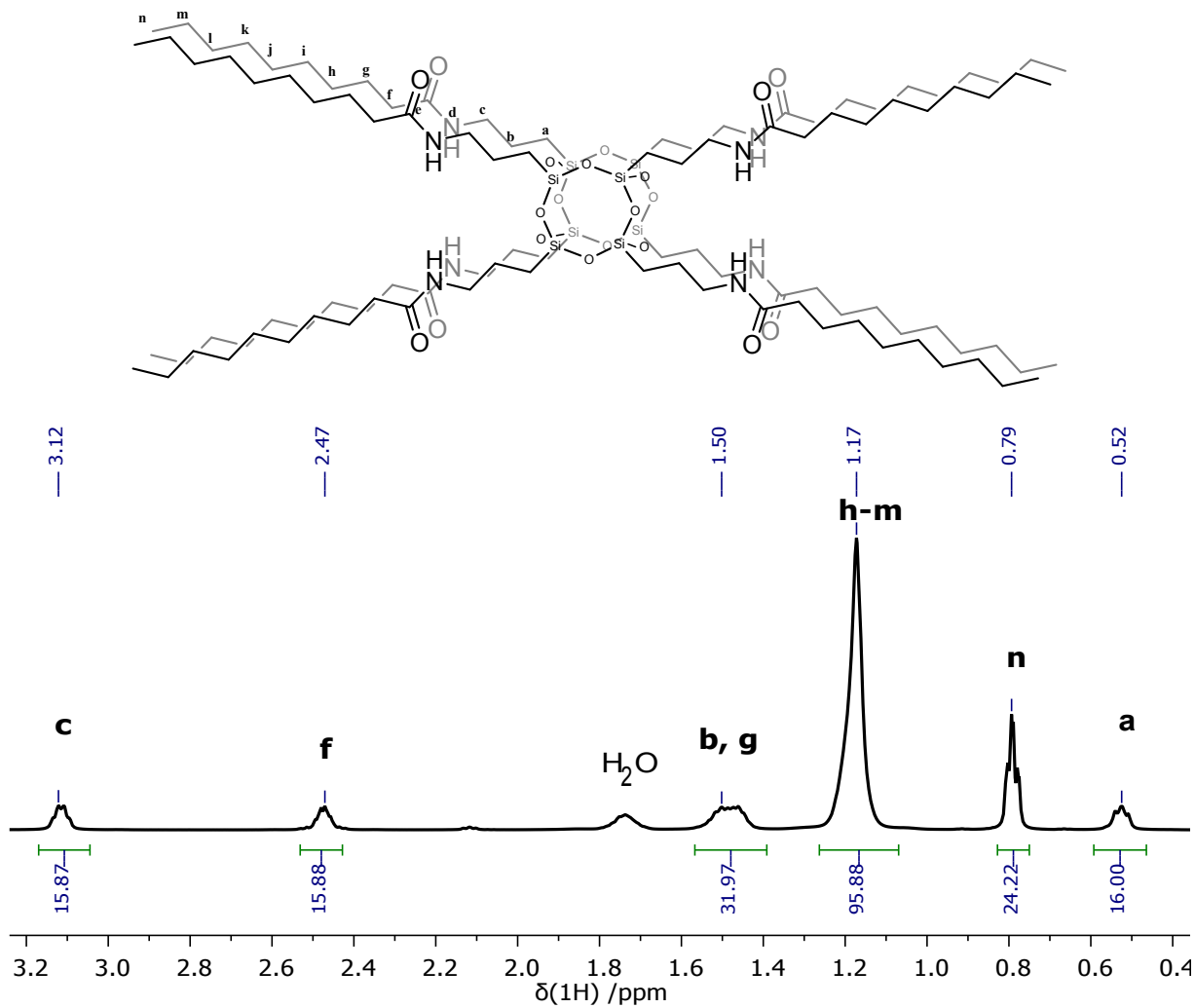


**Figure S31.**  $^1\text{H}$  NMR (500 MHz,  $\text{CDCl}_3$ , 300 K) spectrum of **4**.

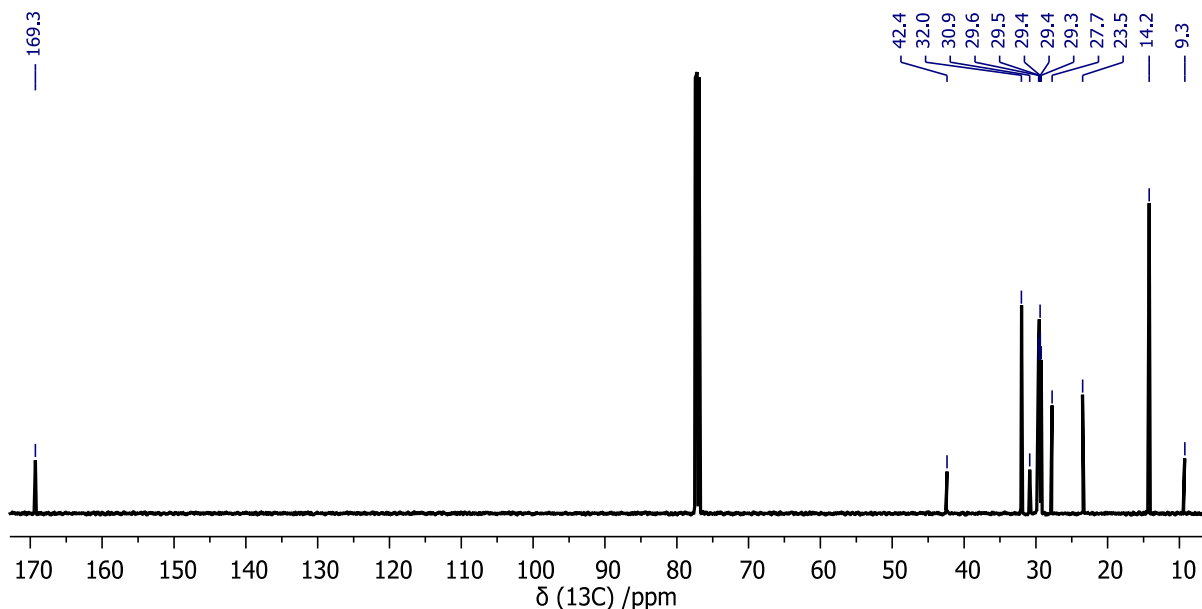
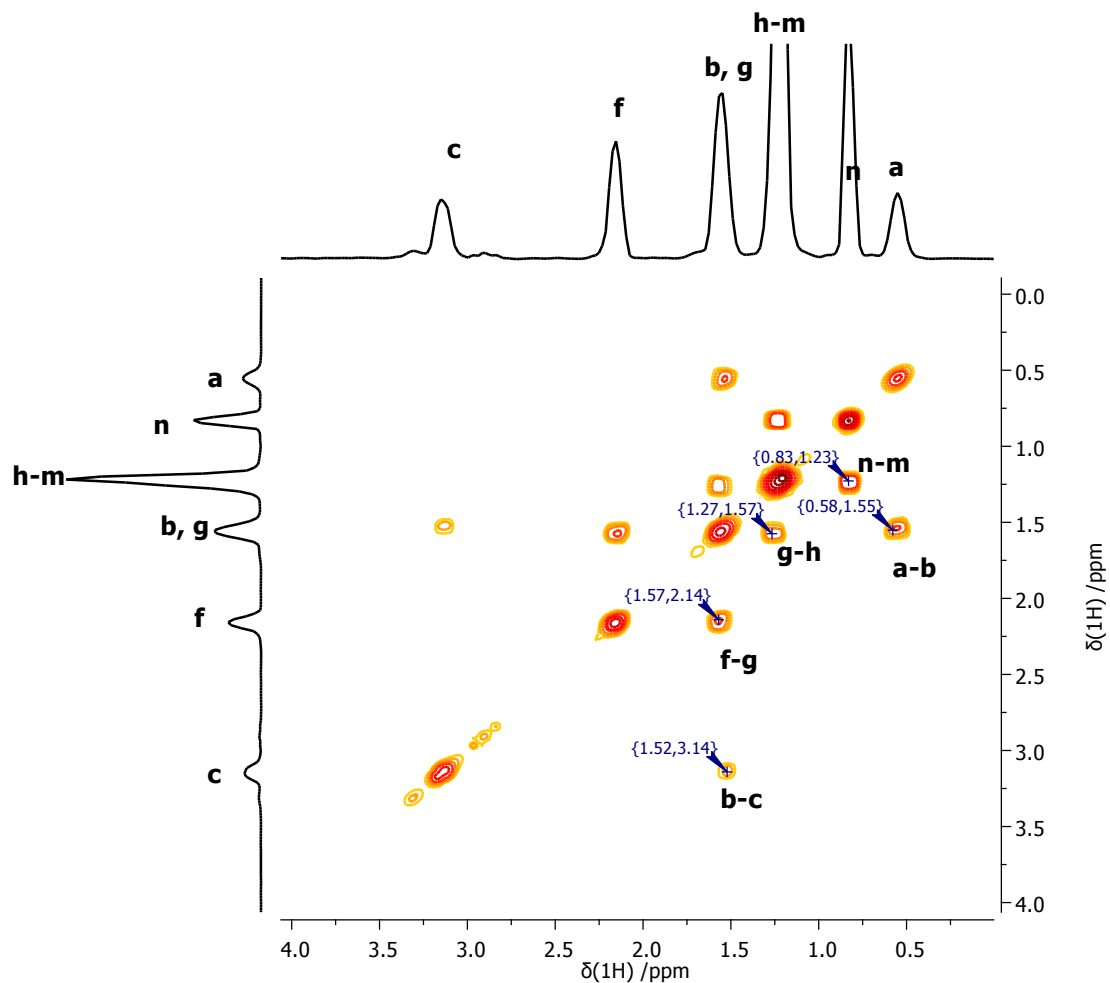


**Figure S32.**  $^{13}\text{C}$  NMR (126 MHz,  $\text{CDCl}_3$ , 300 K) spectrum of **4**.



**Figure**

e S33.  $^1\text{H}$ - $^1\text{H}$  COSY NMR (500 MHz,  $\text{DMSO-d}_6$ , 300 K) spectrum of 4.

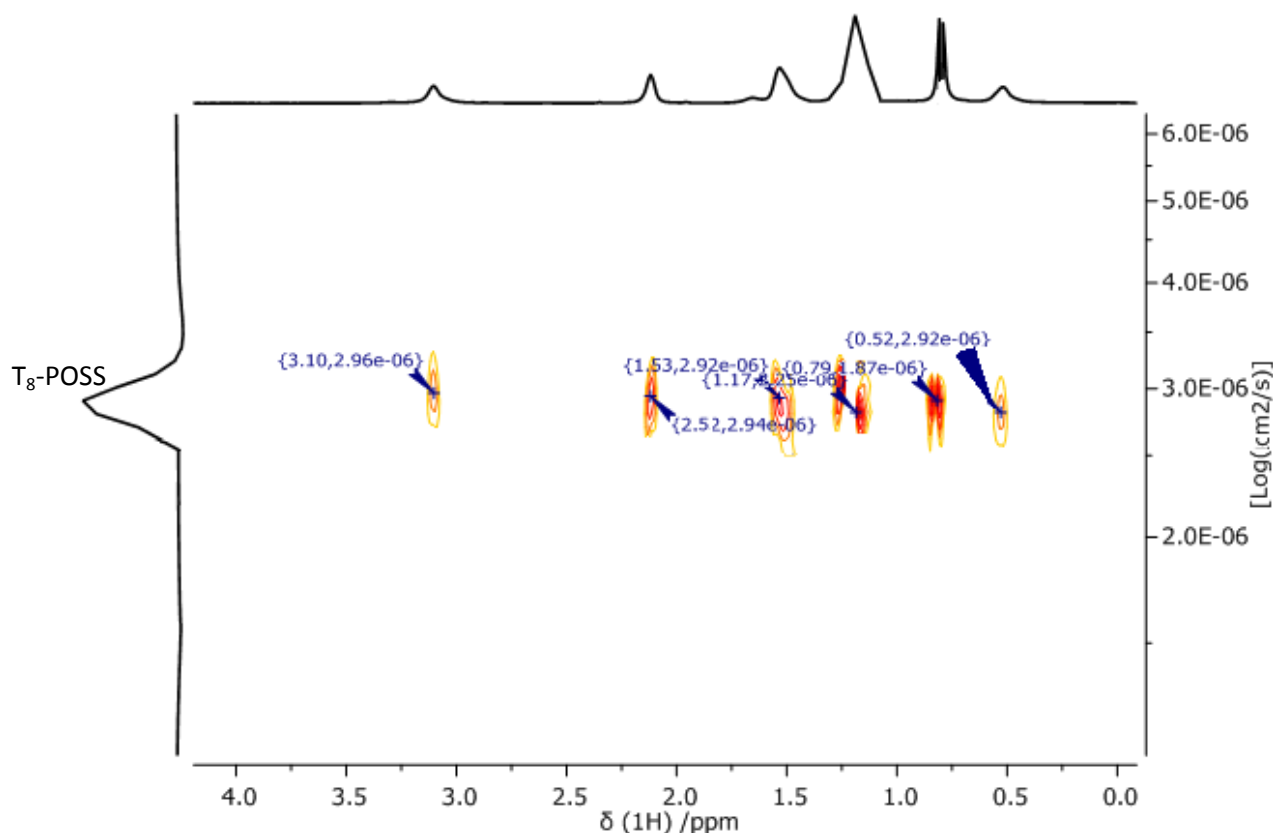


**Figure S34.**  $^1\text{H}$  DOSY (600 MHz,  $\text{CDCl}_3$ , 300 K) spectrum of 4.

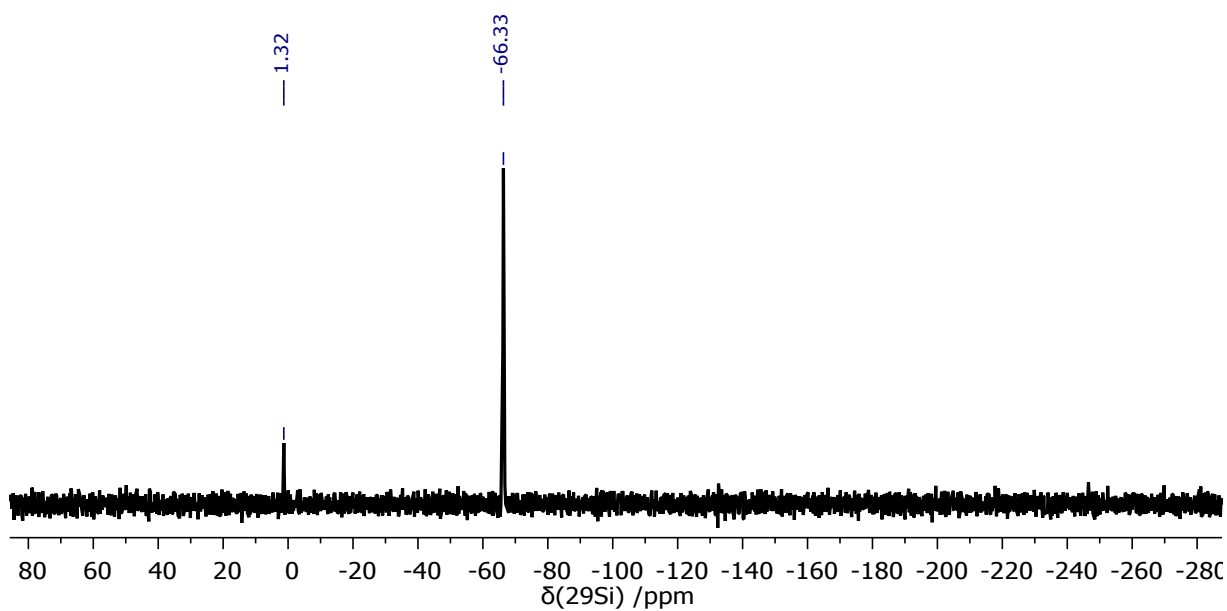


**Figure S35.**  $^{29}\text{Si}$  NMR (59.6 MHz, DMSO-d<sub>6</sub>, 300 K) spectrum of **4**. Chemical shifts were referenced to 4,4-dimethyl-4-silapentane-1-sulfonic acid (DSS) ( $\delta$  1.316).

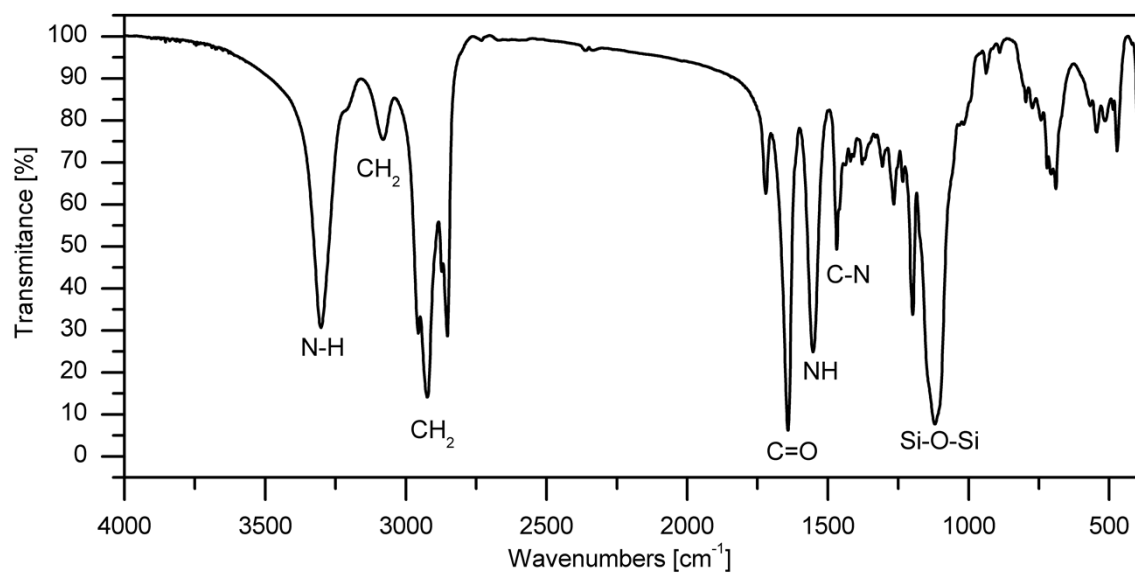


**Figure S36.** FT-IR (KBr pellets) spectrum of **4**.

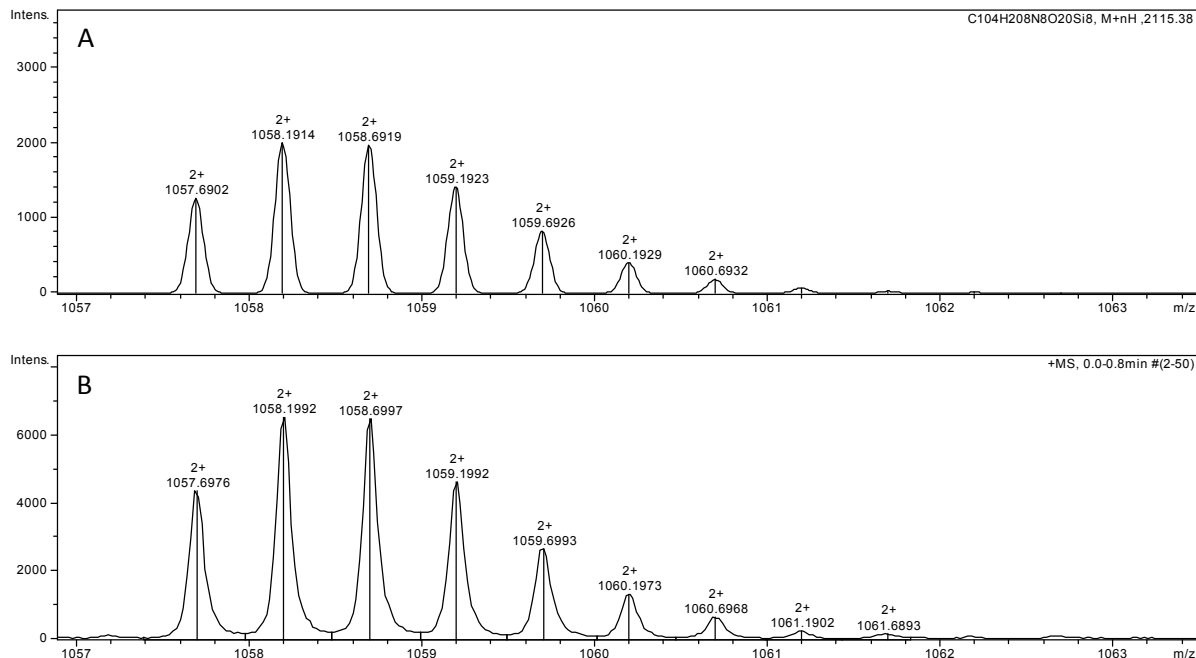


**Figure S37.** Simulated (A) calcd for  $C_{104}H_{210}N_8O_{20}Si_8$ ,  $[M + 2H]^{2+}$  and measured (B) HR-MS (ESI+, TOF,  $CHCl_3$ ) spectra of **4**.

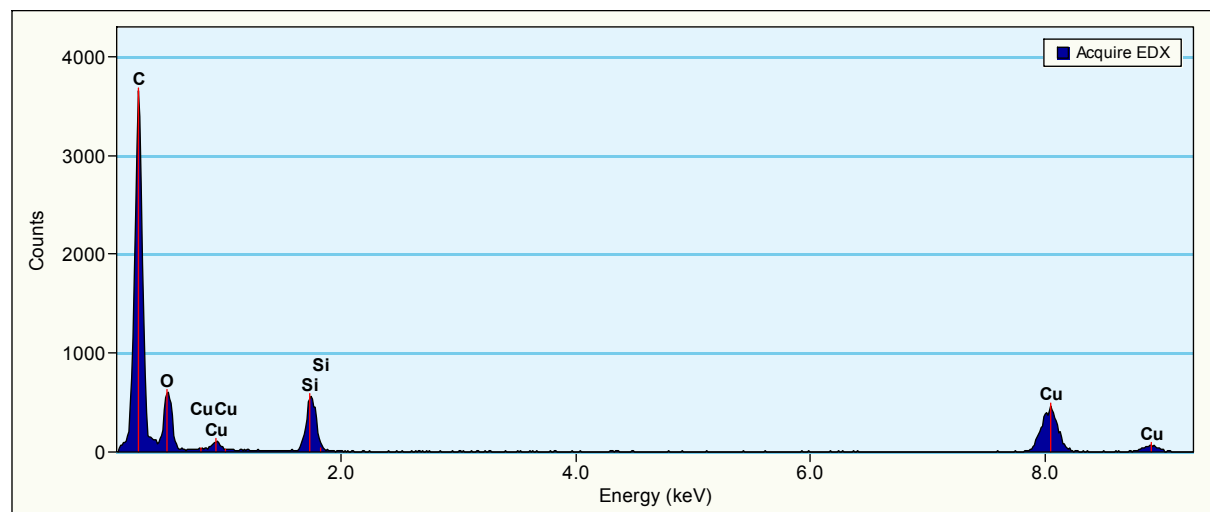


**Figure S38.** EDS spectrum of **4** (copper content is derived from the high-purity conducting Cu grid).

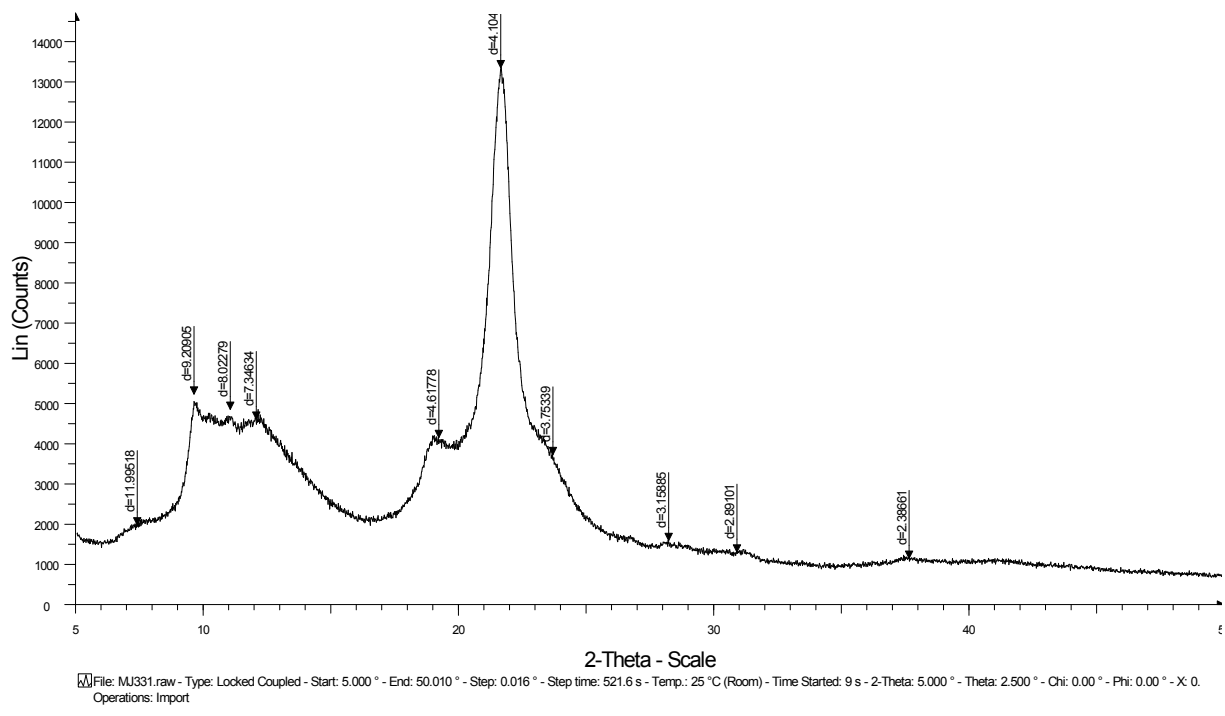


**Figure S39.** Powder XRD pattern of 4.

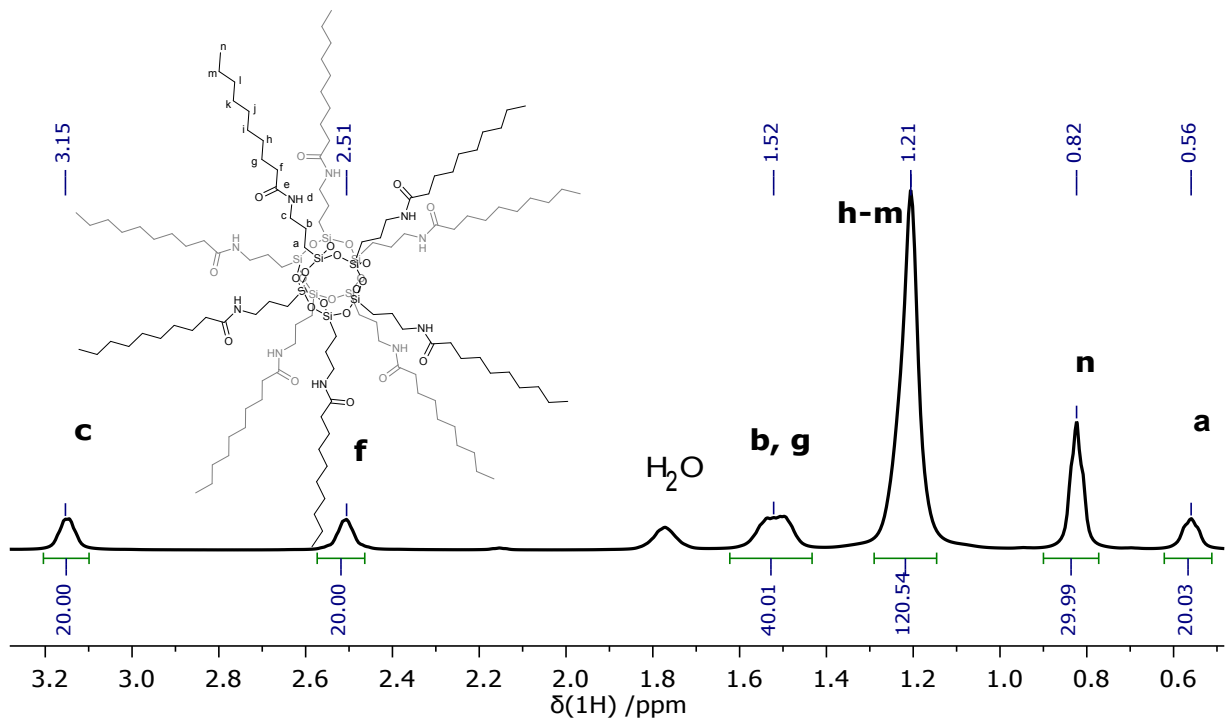


**Figure S40.**  $^1\text{H}$  NMR (500 MHz,  $\text{CDCl}_3$ , 300 K) spectrum of **5**.

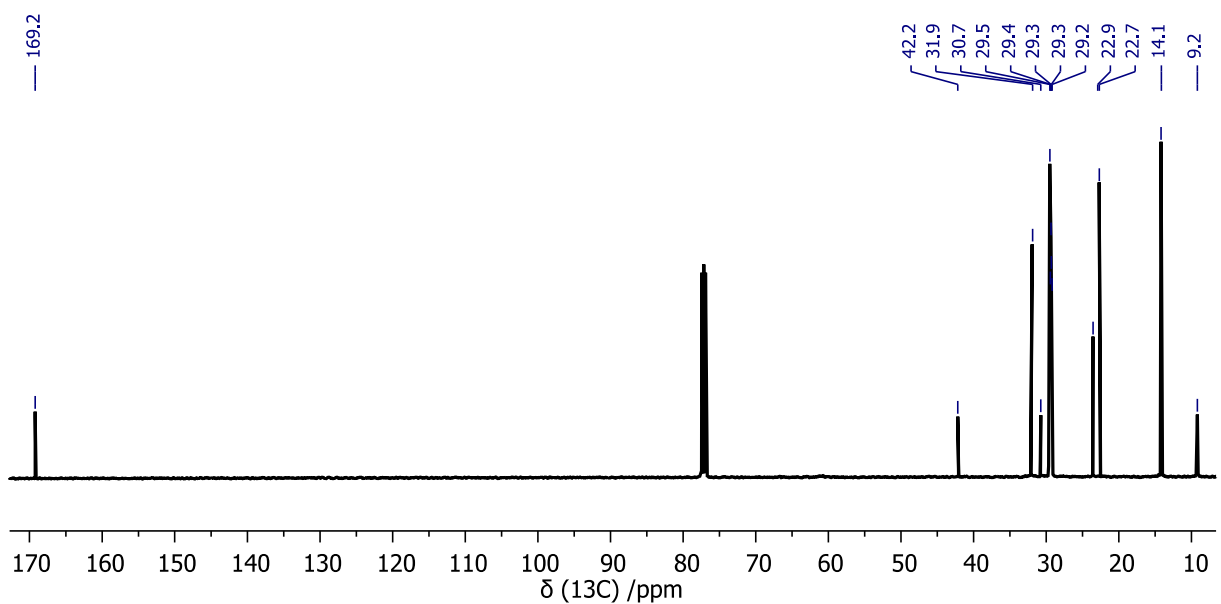


**Figure S41.**  $^{13}\text{C}$  NMR (126 MHz,  $\text{CDCl}_3$ , 300 K) spectrum of **5**.

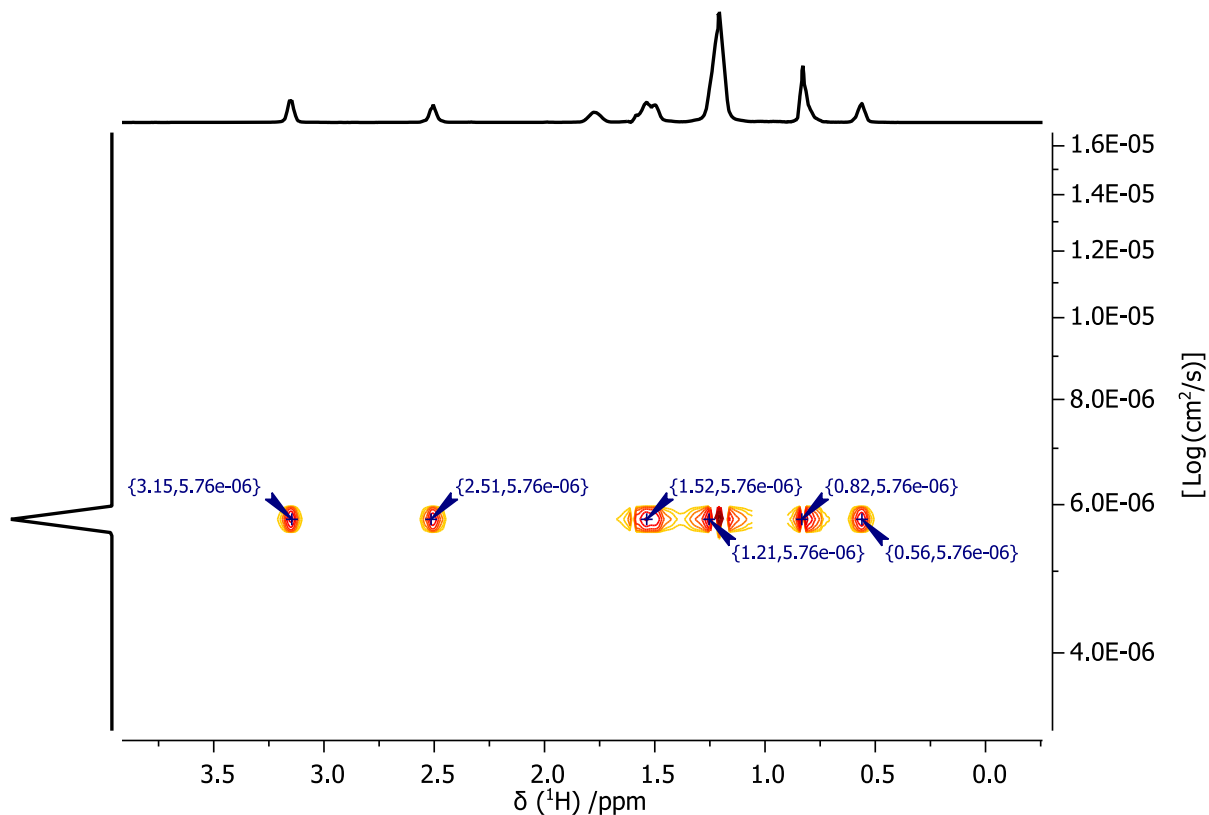


**Figure S42.** <sup>1</sup>H DOSY (600 MHz, CDCl<sub>3</sub>, 300 K) spectrum of **5**.

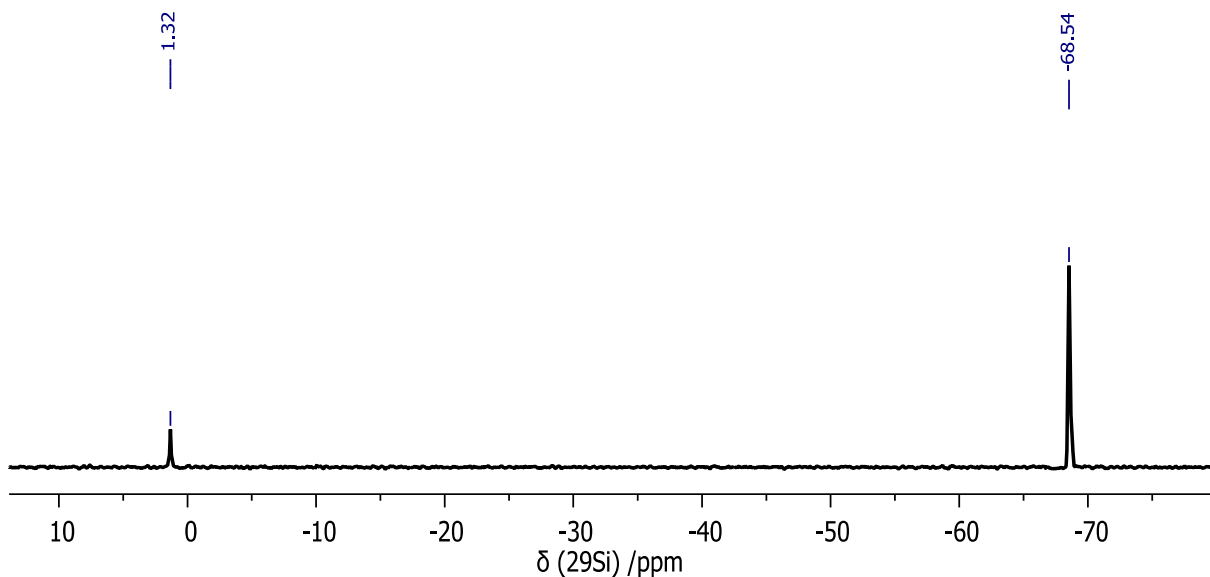


**Figure S43.** <sup>29</sup>Si NMR (59.6 MHz, DMSO-d<sub>6</sub>, 300 K) spectrum of **5**. Chemical shifts were referenced to 4,4-dimethyl-4-silapentane-1-sulfonic acid (DSS) ( $\delta$  1.316).

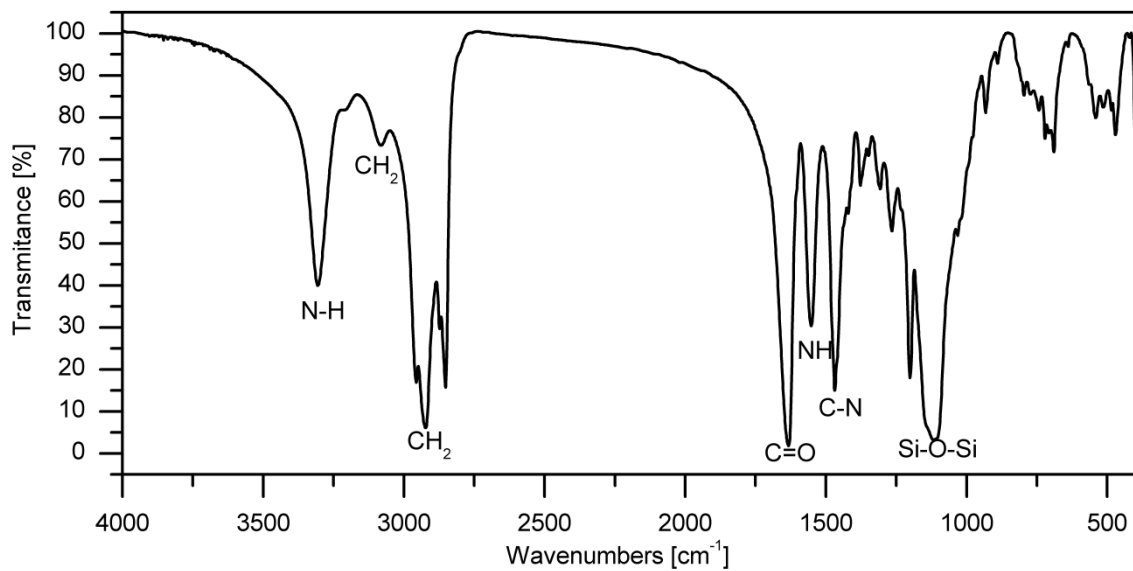


**Figure S44.** FT-IR (KBr pellets) spectrum of **5**.

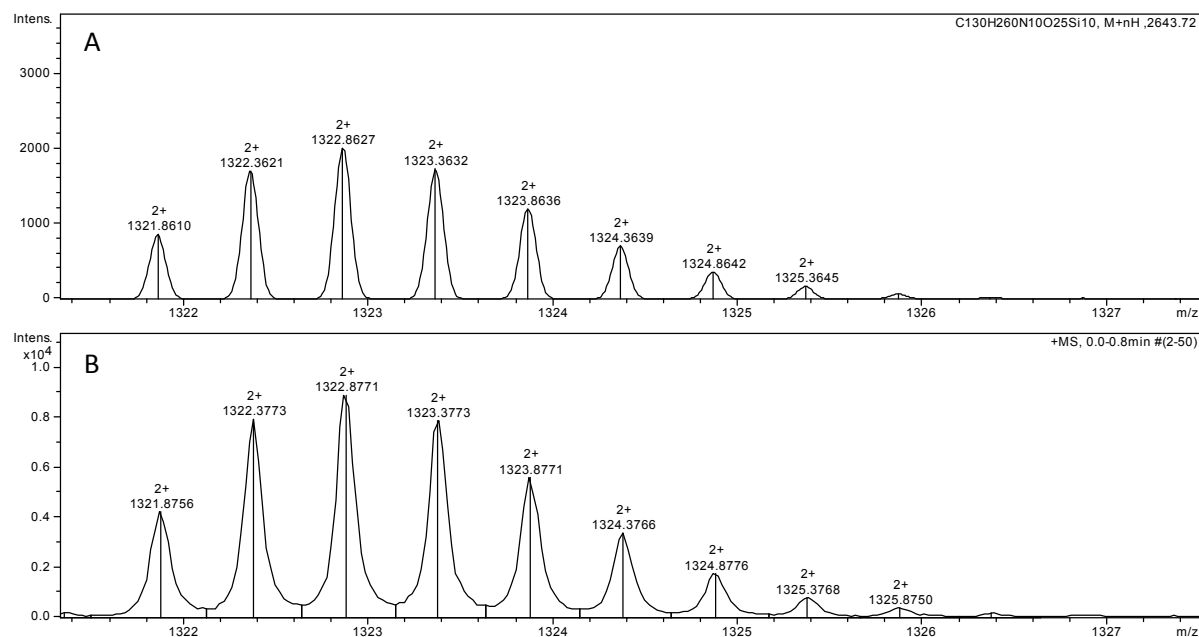
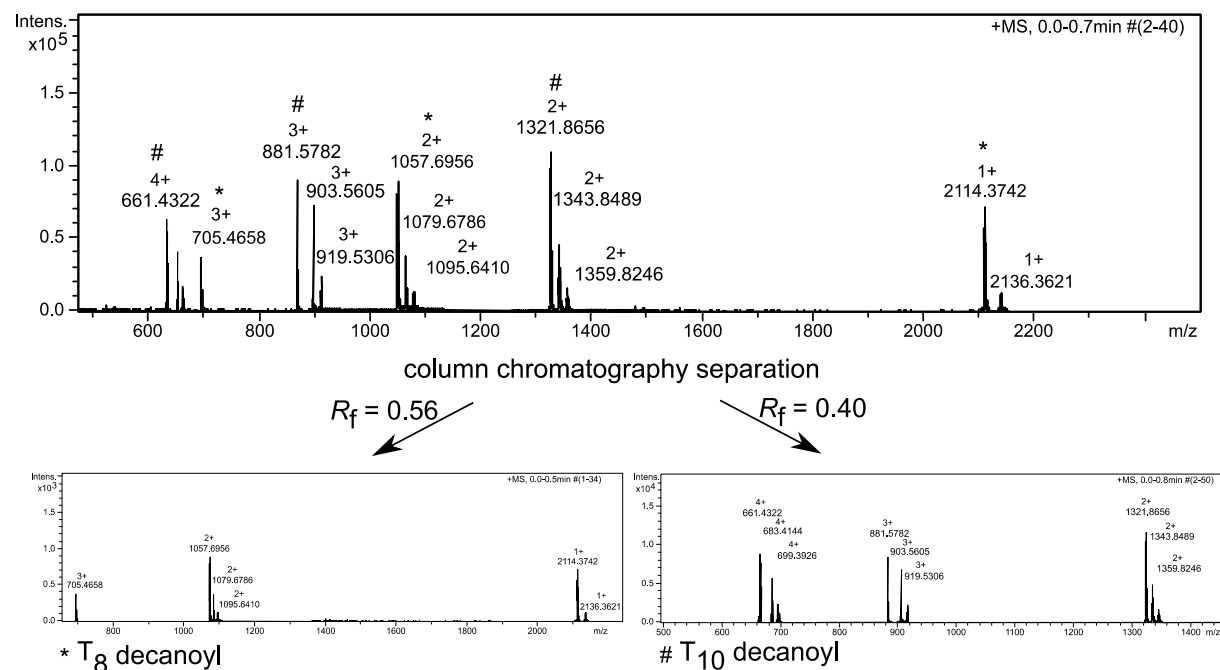


**Figure S45.** Simulated (**A**) calcd for  $\text{C}_{130}\text{H}_{260}\text{N}_{10}\text{O}_{25}\text{Si}_{10}$ ,  $[\text{M} + 2\text{H}]^{2+}$  and measured (**B**) HR-MS (ESI+, TOF,  $\text{CHCl}_3$ ) spectra of **5** (method A).



T <sub>8</sub>			
ion assignment	calcd [m/z]	observed [m/z]	error [ppm]
$[\text{M}+\text{H}]^+$	2114.3732	2114.3742	-0.5
$[\text{M}+2\text{H}]^{2+}$	1057.6902	1057.6956	5
$[\text{M}+3\text{H}]^{3+}$	705.4626	705.4658	5
$[\text{M}+\text{Na}]^+$	2136.3551	2136.3621	3
$[\text{M}+2\text{Na}]^{2+}$	1079.6721	1079.6786	6
$[\text{M}+2\text{K}]^{2+}$	1095.6461	1095.6410	-5

T <sub>10</sub>			
ion assignment	calcd [m/z]	observed [m/z]	error [ppm]
$[\text{M}+2\text{H}]^{2+}$	1321.8610	1321.8656	3
$[\text{M}+3\text{H}]^{3+}$	881.5764	881.5782	2
$[\text{M}+4\text{H}]^{4+}$	661.4341	661.4322	-3
$[\text{M}+2\text{Na}]^{2+}$	1343.8429	1343.8489	4
$[\text{M}+3\text{Na}]^{3+}$	903.5583	903.5605	2
$[\text{M}+4\text{Na}]^{4+}$	683.4161	683.4144	-2
$[\text{M}+2\text{K}]^{2+}$	1359.8168	1359.8246	6
$[\text{M}+3\text{K}]^{3+}$	919.5323	919.5306	-2
$[\text{M}+4\text{K}]^{4+}$	699.3900	699.3926	4

**Figure S46.** HR-MS (ESI+, TOF,  $\text{CHCl}_3$ ) spectra of **4** and **5**.

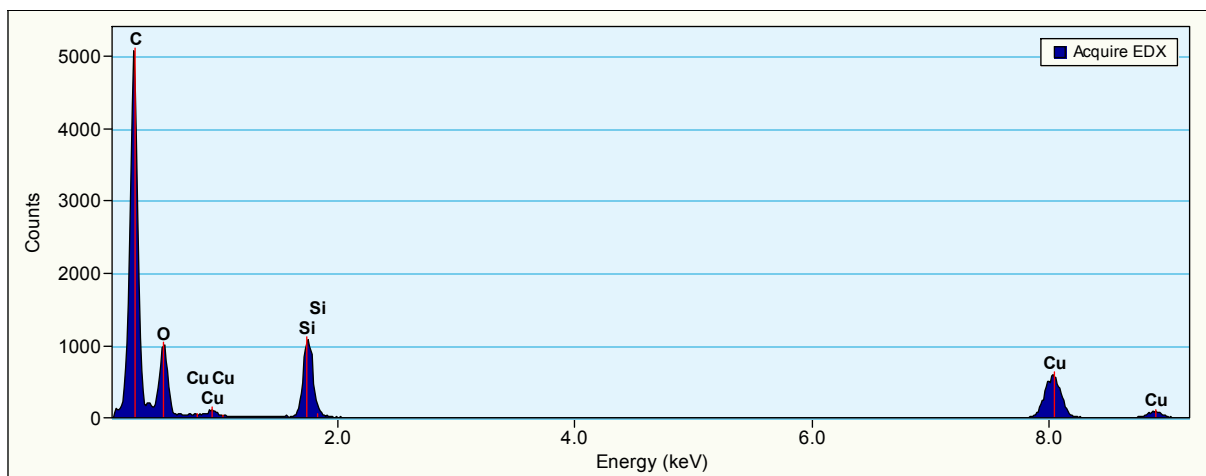


**Figure S47.** EDS spectrum of **5** (copper content is derived from the high-purity conducting Cu grid).

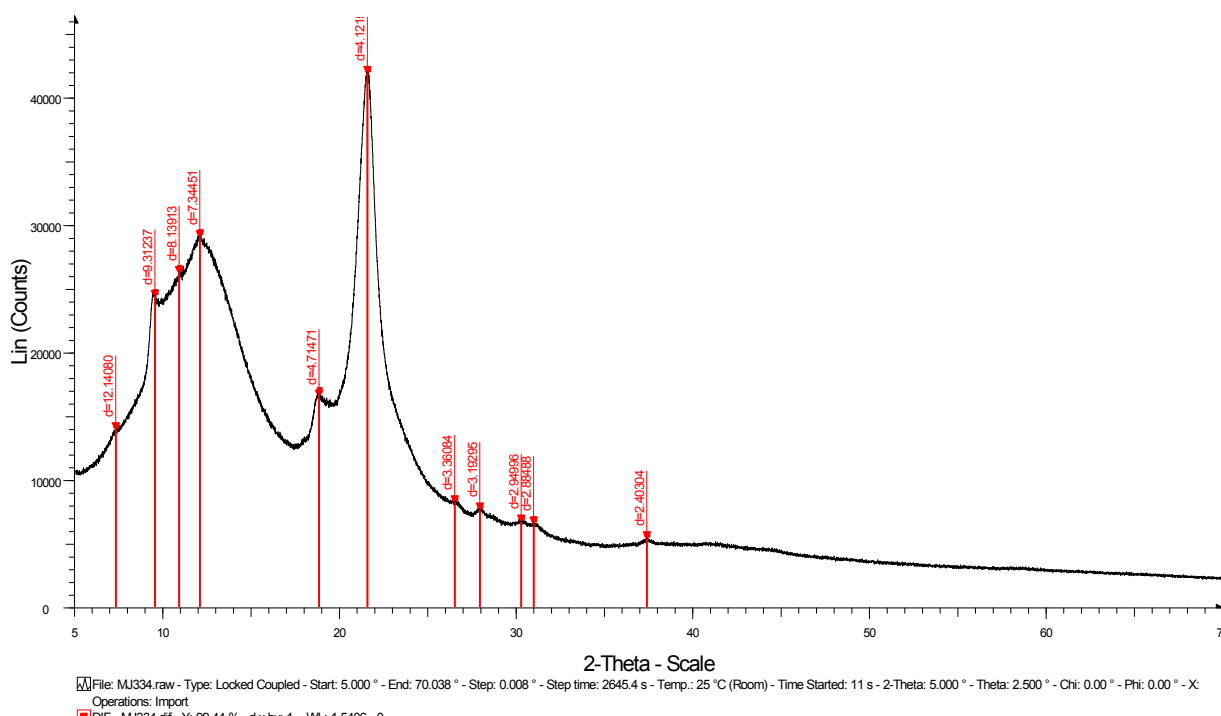


**Figure S48.** Powder XRD pattern of **5**.

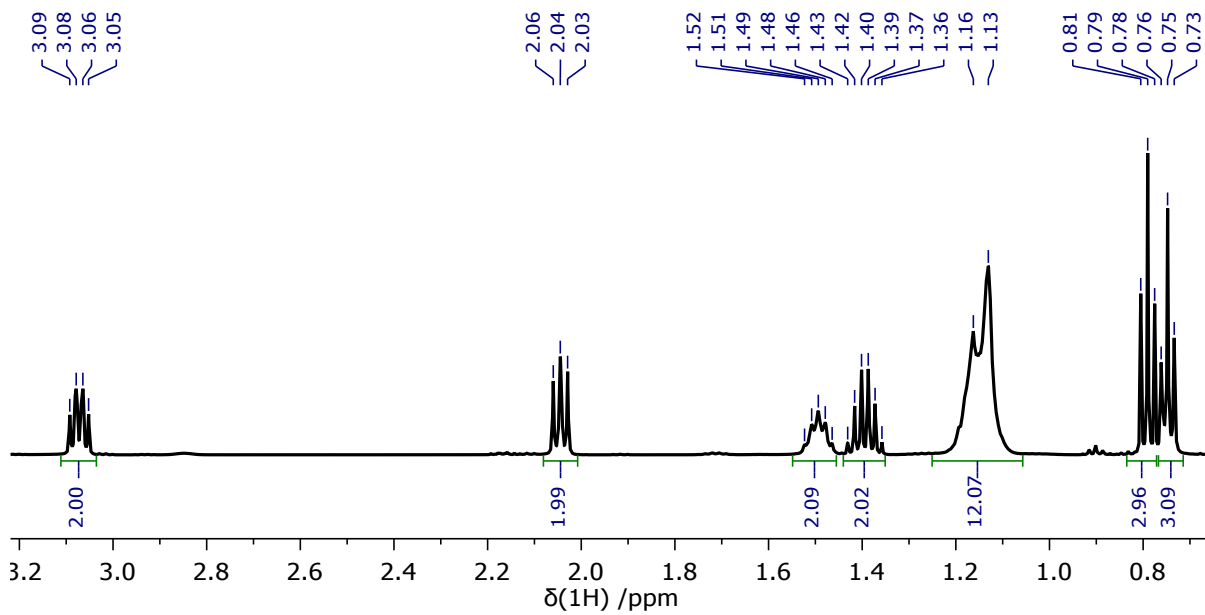


**Figure S49.**  $^1\text{H}$  NMR (500 MHz,  $\text{CDCl}_3$ , 300 K) spectrum of **6**.

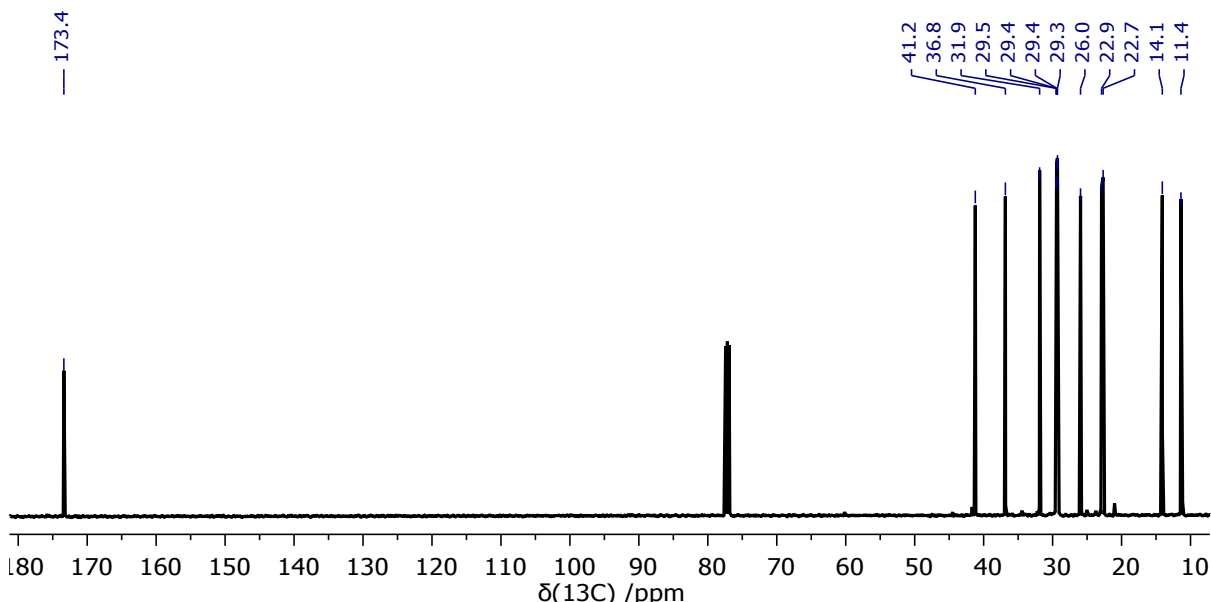


**Figure S50.**  $^{13}\text{C}$  NMR (126 MHz,  $\text{CDCl}_3$ , 300 K) spectrum of **6**.

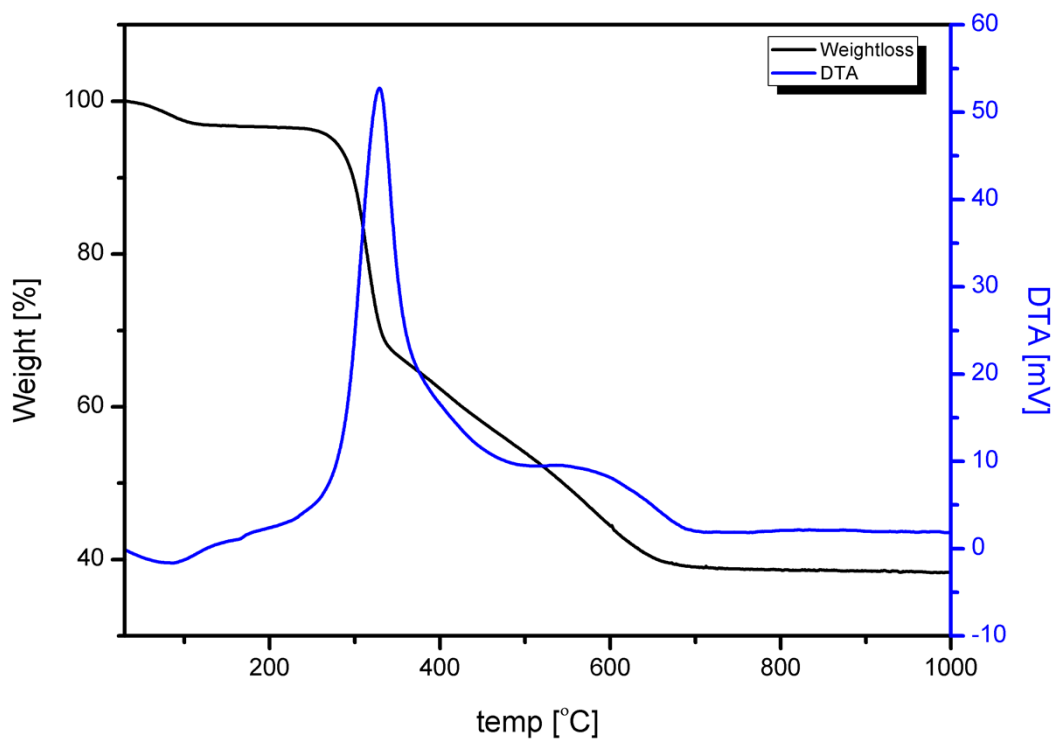


**Figure S51.** TG (black line), and DTA (blue line) thermogram of **1** 10 °C/min (in the air atmosphere: 60% N<sub>2</sub>, 40% O<sub>2</sub>).

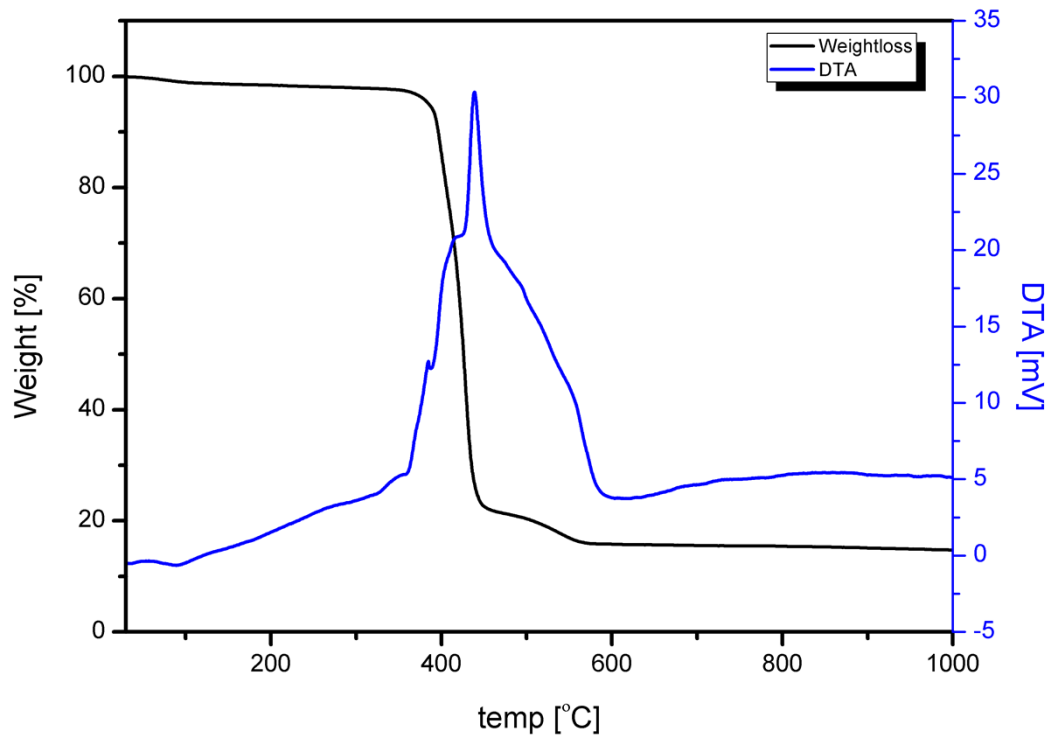


**Figure S52.** TG (black line), and DTA (blue line) thermogram of **2** 10 °C/min (in the air atmosphere: 60% N<sub>2</sub>, 40% O<sub>2</sub>).

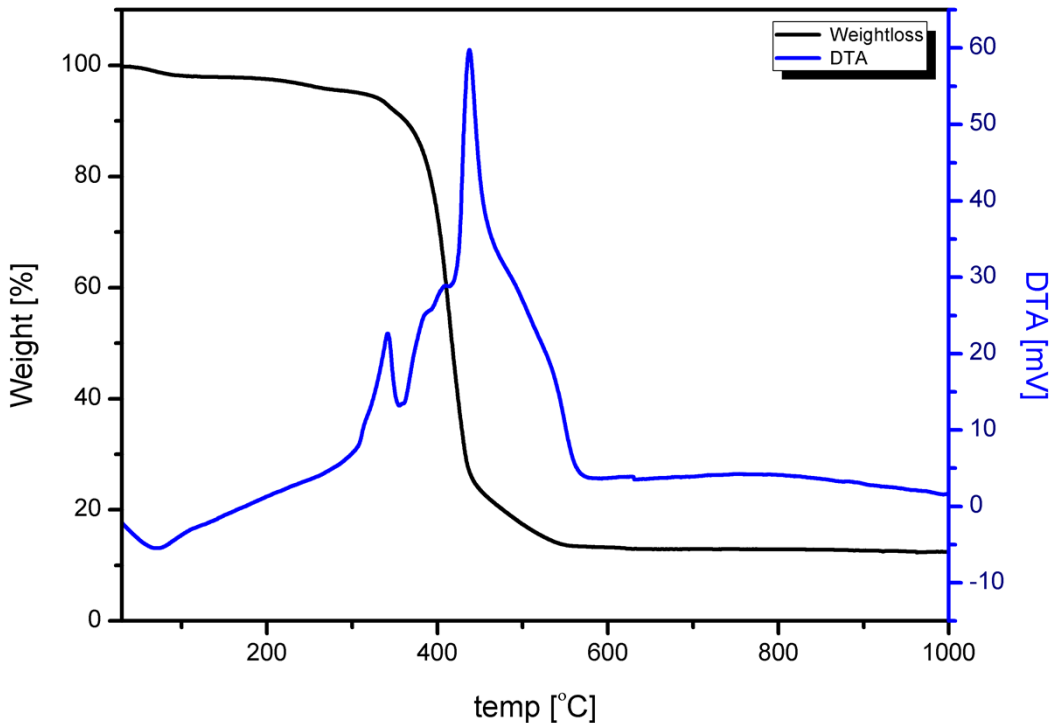


**Figure S53.** TG (black line), and DTA (blue line) thermogram of **3** 10 °C/min (in the air atmosphere: 60% N<sub>2</sub>, 40% O<sub>2</sub>).

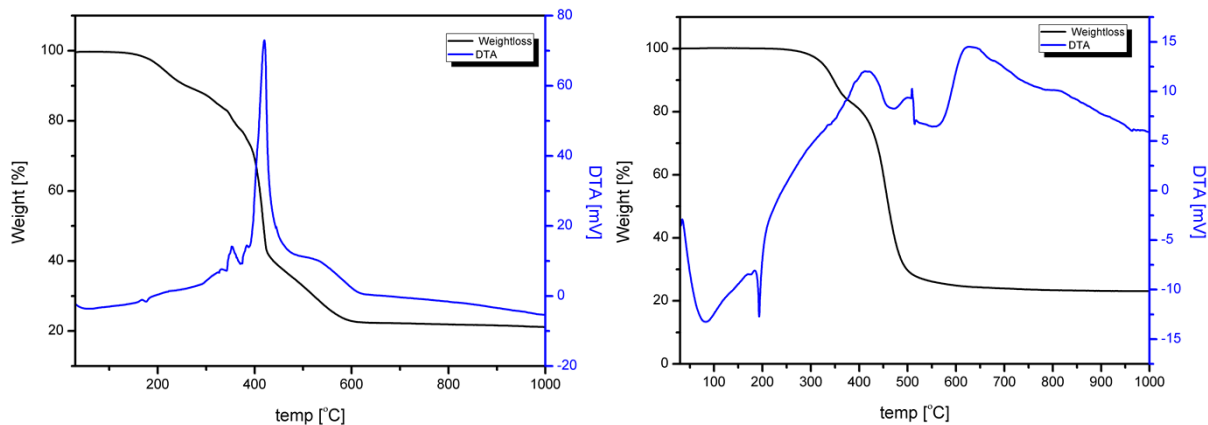


**Figure S54.** TG (black line), and DTA (blue line) thermogram of **4** 10 °C/min. Left graph in the air atmosphere (60% N<sub>2</sub>, 40% O<sub>2</sub>), right in nitrogen.

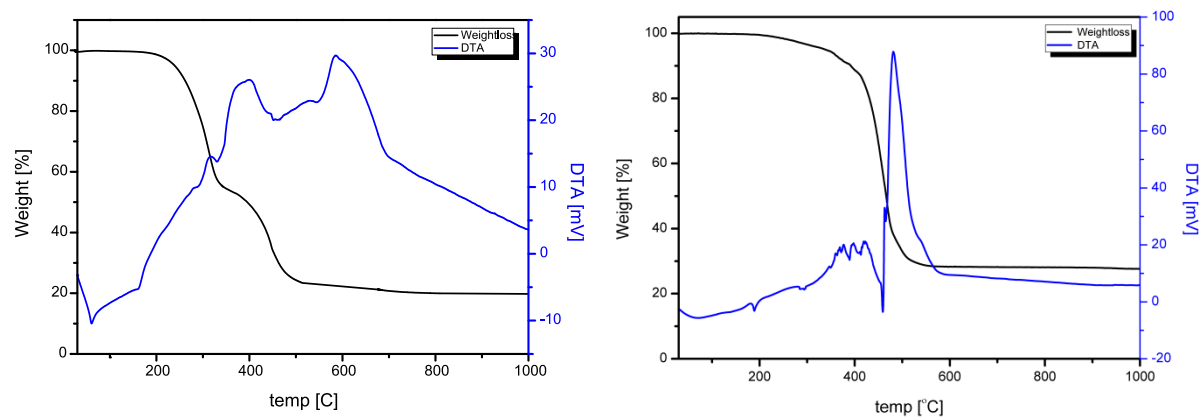


**Figure S55.** TG (black line), and DTA (blue line) thermogram of **5** 10 °C/min. Left graph in the air atmosphere (60% N<sub>2</sub>, 40% O<sub>2</sub>), right in nitrogen.

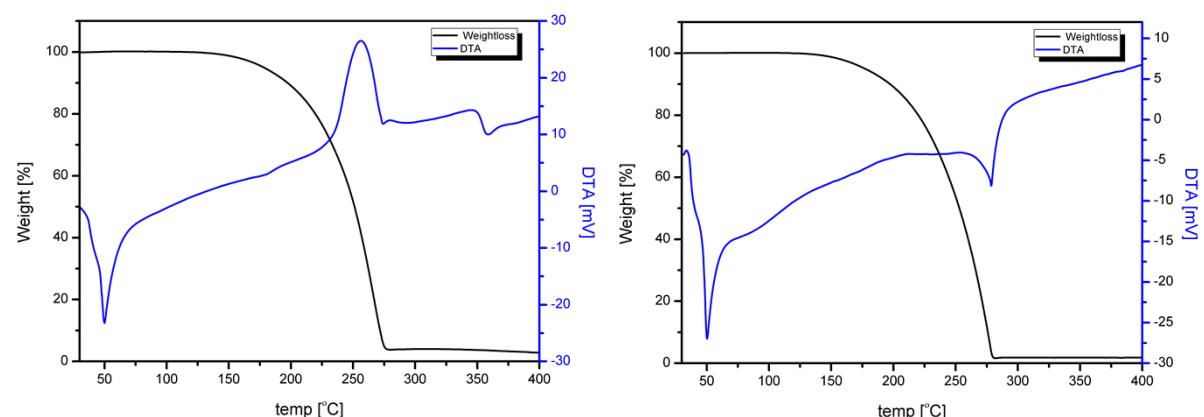


**Figure S56.** TG (black line), and DTA (blue line) thermogram of **6** 10 °C/min. Left graph in the air atmosphere (60% N<sub>2</sub>, 40% O<sub>2</sub>), right in nitrogen.

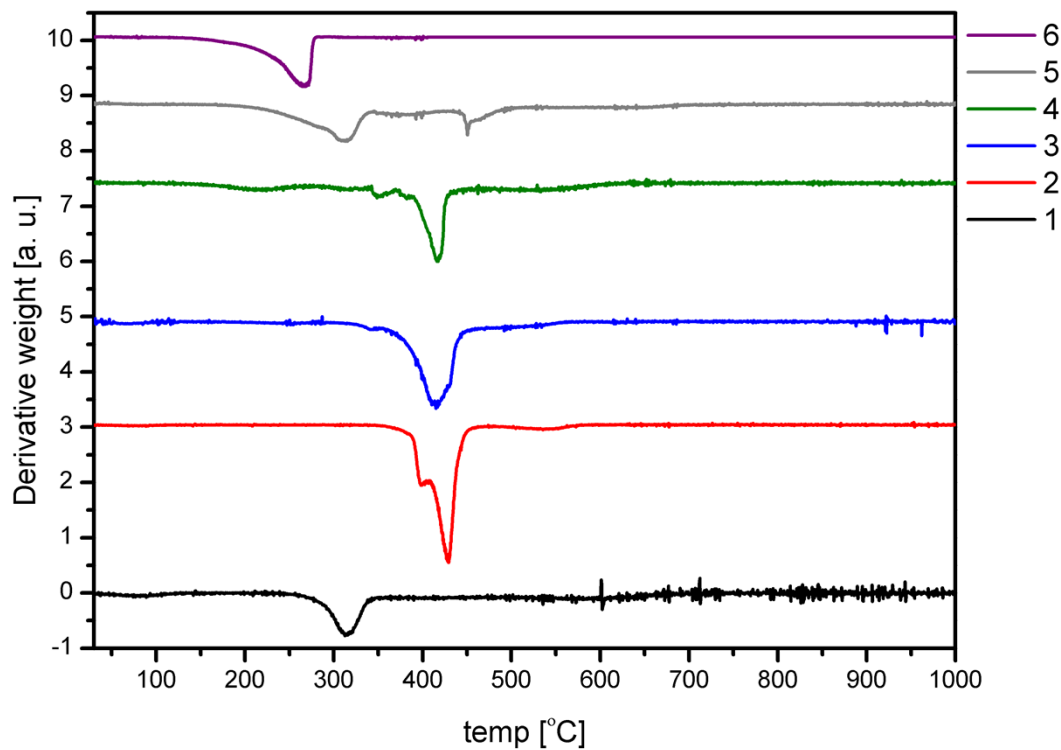


**Figure S57.** First derivative of TG (DTG) thermograms of **1–6** 10 °C/min (in the air atmosphere: 60% N<sub>2</sub>, 40% O<sub>2</sub>).

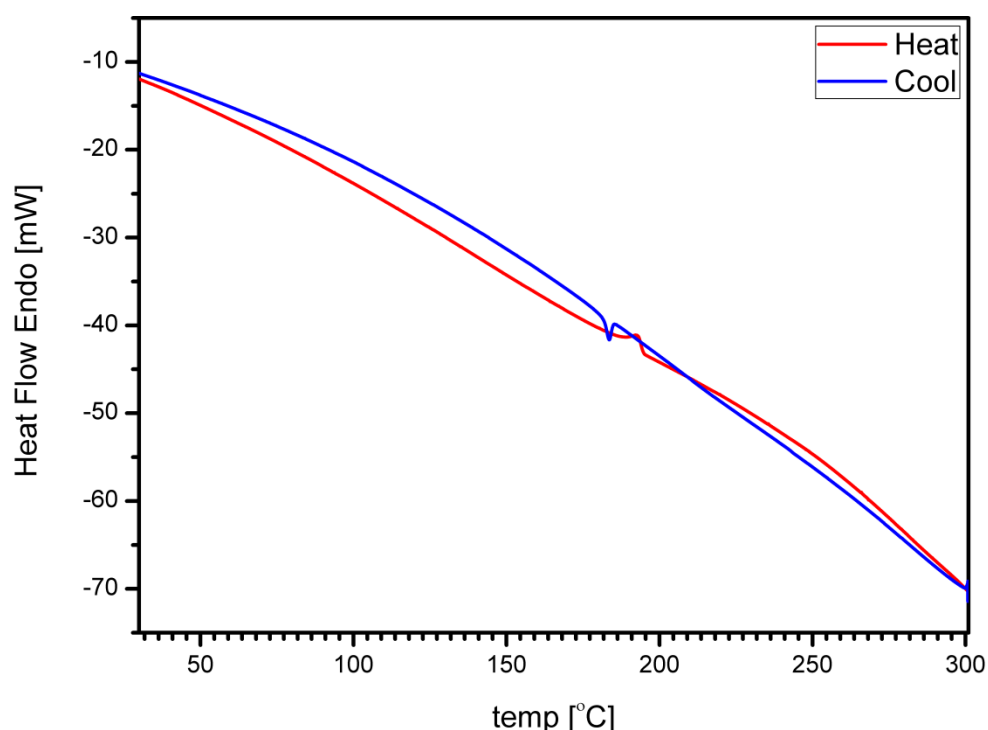


**Figure S58.** DSC of **5**, 2<sup>nd</sup> heat & cooling cycle (5 °C/min in the nitrogen atmosphere).

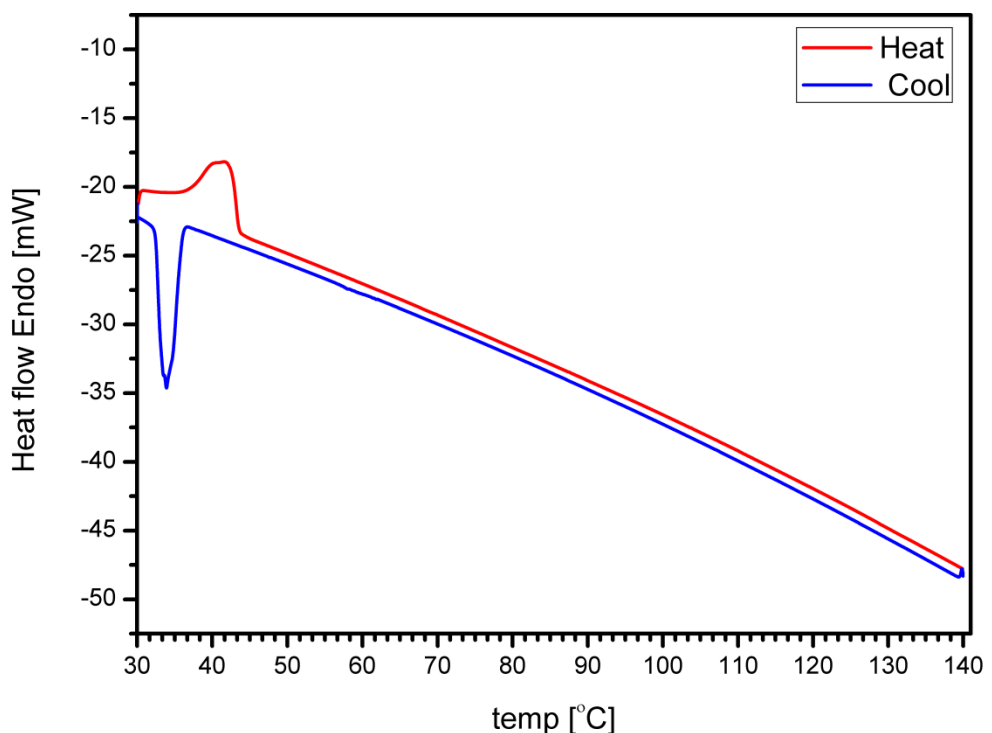


**Figure S59.** DSC of **6**, 2<sup>nd</sup> heat & cooling cycle (5 °C/min in the nitrogen atmosphere).

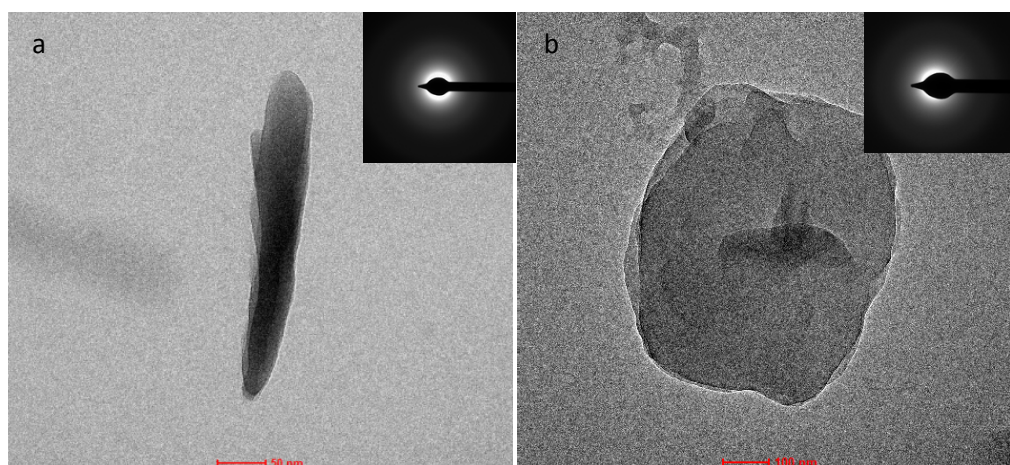


**Figure S60.** Selected HR-TEM images of **4** (a) and **5** (b).

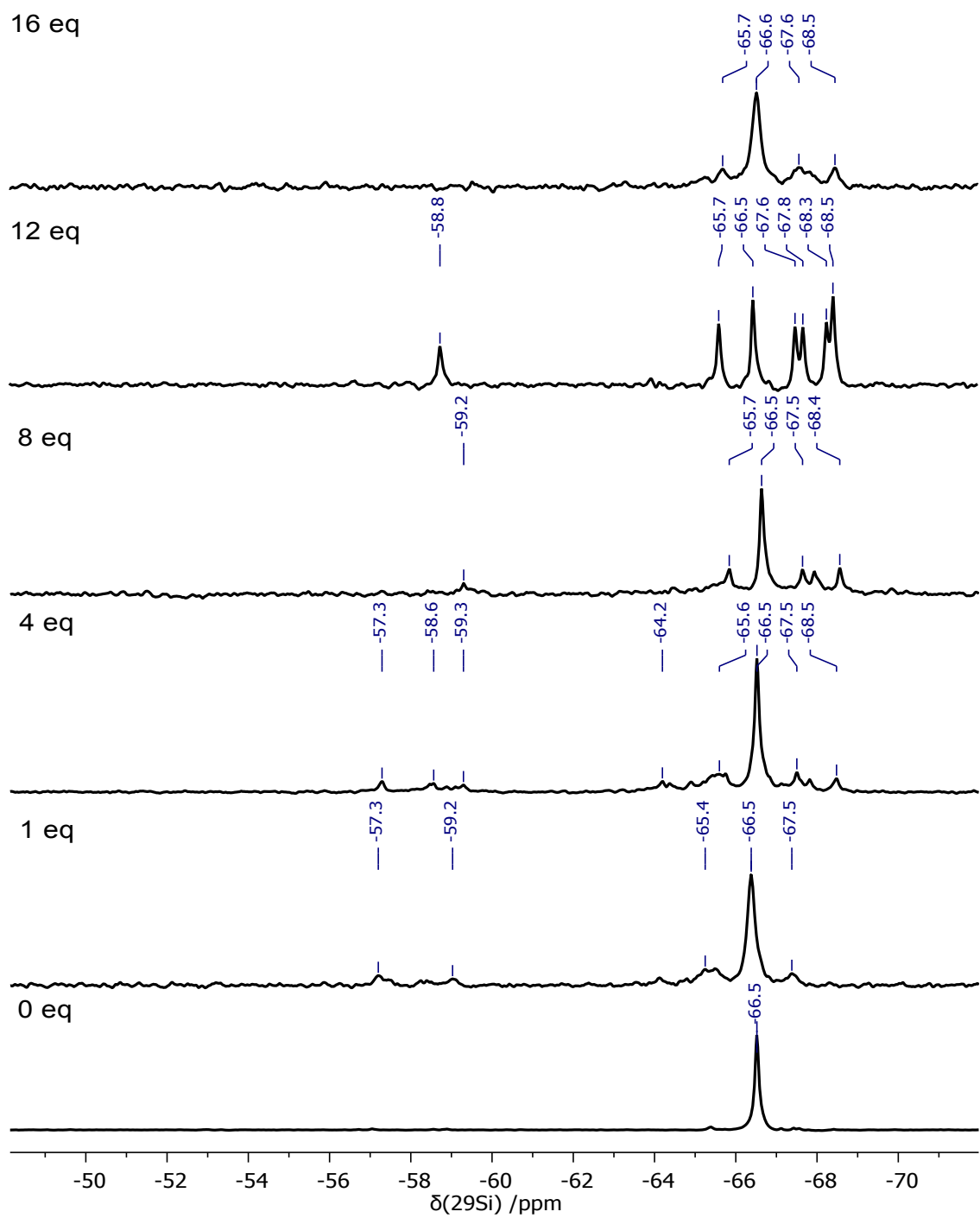


**Figure S61.**  $^{29}\text{Si}$  NMR (59.6 MHz,  $\text{DMSO-d}_6$ , 300 K) spectrum of **1** after reaction with 0, 1, 4, 8, 12 and 16 equivalents of  $\text{CH}_3\text{SO}_3\text{H}$ . Chemical shifts were referenced to tetramethylsilane (TMS).

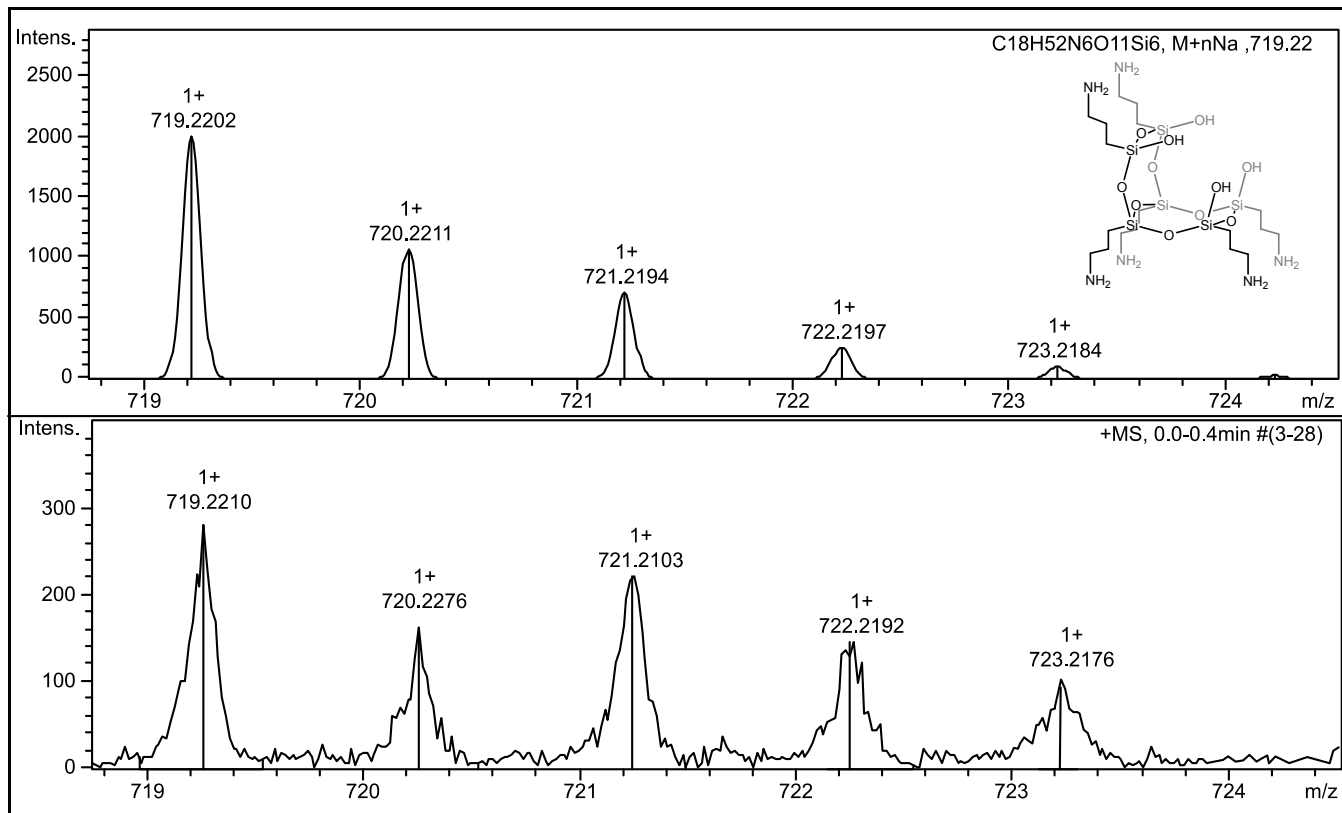


**Figure S62.** Simulated (up) calcd for  $\text{C}_{18}\text{H}_{52}\text{N}_6\text{O}_{11}\text{Si}_6\text{Na}$ ,  $[\text{M} + \text{Na}]^+$  and measured (down) HR-MS (ESI+, TOF, MeOH) spectra of **C**.

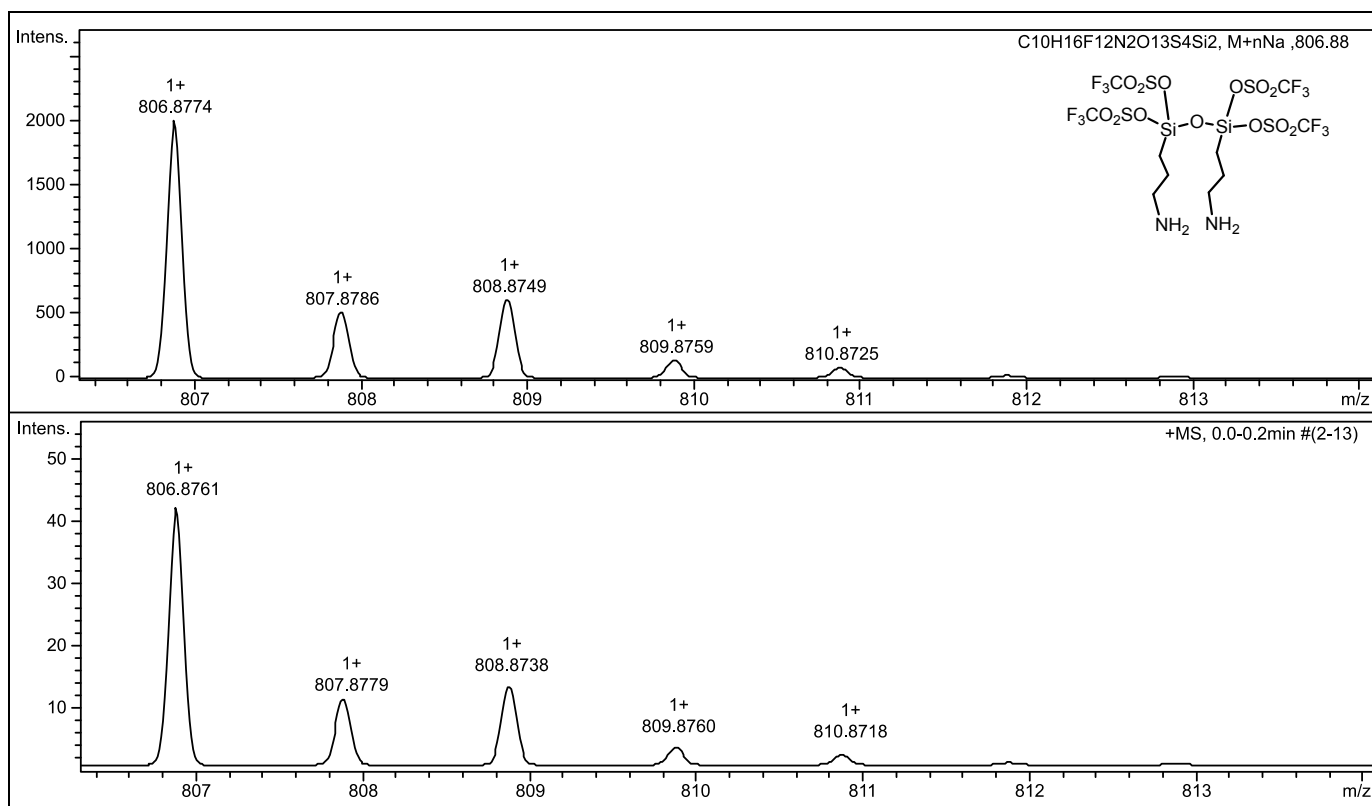


**Figure S63.** Simulated (up) calcd for  $\text{C}_{10}\text{H}_{16}\text{F}_{12}\text{N}_2\text{O}_{13}\text{S}_4\text{Si}_2\text{Na}$ ,  $[\text{M} + \text{Na}]^+$  and measured (down) HR-MS (ESI+, TOF, MeOH) spectra of **D**.

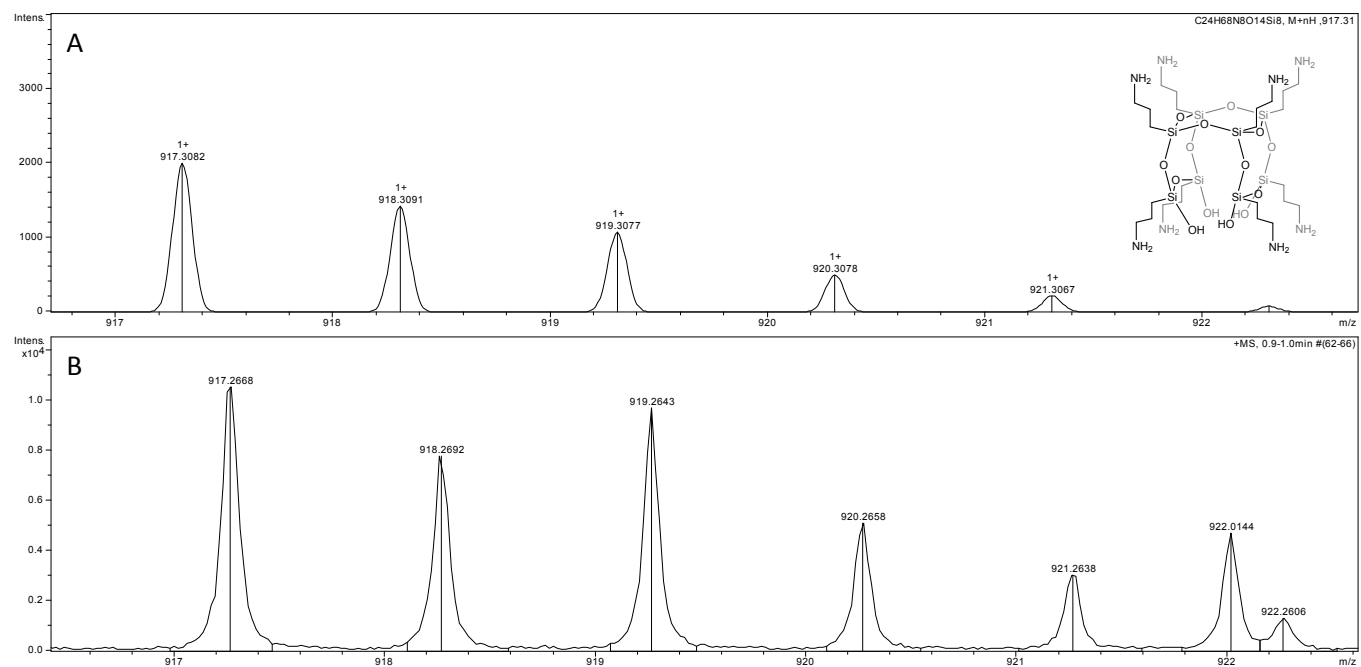


**Figure S64.** Simulated (up) calcd for  $C_{24}H_{68}N_8O_{14}Si_8$ ,  $[M + H]^+$  and measured (down) HR-MS (ESI+, TOF, MeOH) spectra of **E**.

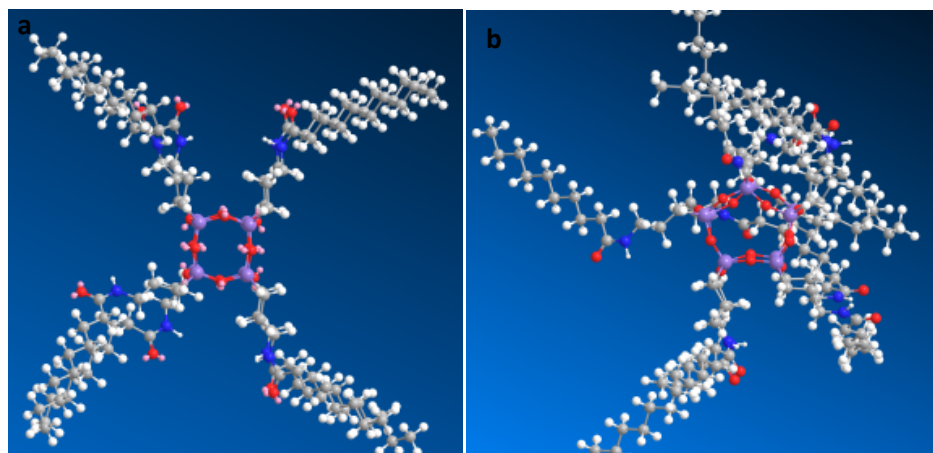


**Figure S65.** Molecular models of compound 4 (a), compound 5 (b).

**Table S1.** MM2 calculations of the minimization energies of Compound **2**, **3**, **4**, **5**.

Energy parameters*	Amine		Amide	
	Compound <b>2</b>	Compound <b>3</b>	Compound <b>4</b>	Compound <b>5</b>
Stretch:	1.7969	7.6789	7.0276	11.1709
Bend:	7.0679	58.1066	27.8027	155.4612
Stretch-Bend:	-0.6755	-4.5902	0.9053	0.4549
Torsion:	0.9477	3.1937	29.6476	39.5012
Non-1,4 VDW:	-35.4194	-53.9810	-52.8458	-123.3177
1,4 VDW:	2.4715	15.4807	44.0530	66.8356
Dipole/Dipole:	35.5346	35.0298	-25.4860	-47.7560
Total Energy:	11.7237	60.9185	31.1044	102.3501

\*units of energy are kcal/mol

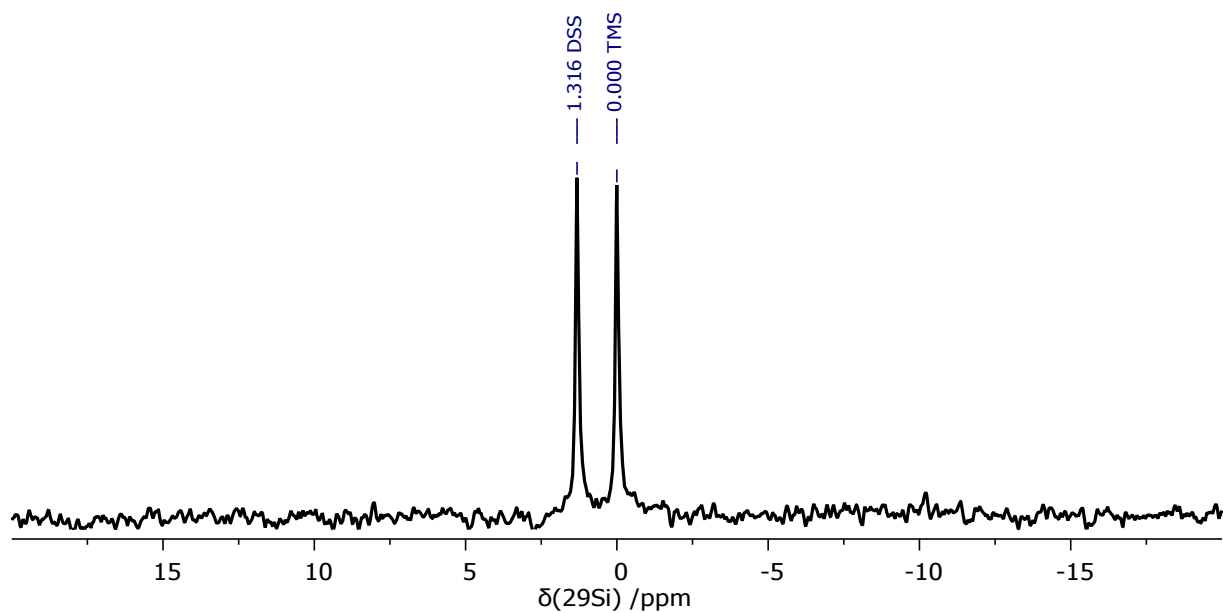


**Figure S66.**  $^{29}\text{Si}$  NMR (59.63 MHz,  $\text{DMSO-d}_6$ , 300 K) spectrum of DSS (4,4-dimethyl-4-silapentane-1-sulfonic acid). Chemical shifts were referenced to TMS (Tetramethylsilane) ( $\delta$  0.000).